# Materials Advances

Accepted Manuscript

This article can be cited before page numbers have been issued, to do this please use: M. Choudhary, N. Chakinala, P. Saini, P. K. Surolia and A. G. Chakinala, *Mater. Adv.*, 2025, DOI: 10.1039/D5MA00720H.




ROYAL SOCIETY OF CHEMISTRY

rsc.li/materials-advances

View Article Online
DOI: 10.1039/D5MA00720H



# Carbon foams derived from biomass with ultra-high adsorption capacity for the removal of tetracycline

Meena Choudhary[a,b], Nandana Chakinala[a,c*], Pooja Saini[a,b], Praveen K. Surolia[b*], Anand Gupta Chakinala[a*]

[a] *Chemical Reaction Engineering Laboratory, Department of Biotechnology & Chemical Engineering, Manipal University Jaipur, Jaipur - 303007, Rajasthan, India.*

[b]*Solar Energy Conversion and Nanomaterial Laboratory, Department of Chemistry, Manipal University Jaipur, Jaipur - 303007, Rajasthan, India.*

[c]*School of Chemistry, University of Leeds, Woodhouse Lane, Leeds, LS2 9JT, UK.*

Tel: +91-7073580885,

*Email: anandgupta.chakinala@jaipur.manipal.edu (Anand Chakinala)

n.chakinala@leeds.ac.uk (Nandana Chakinala)

Praveenkumar.surolia@jaipur.manipal.edu (Praveen Surolia)



## ABSTRACT

This study focusses on the development of carbon foams (CF) derived from carbohydrates evaluated for their adsorptive removal of model pollutants. The influence of different metal nitrates (cobalt, zinc, iron, magnesium, and chromium) and carbon precursors (cellulose, agar, sucrose, and starch) on the CF preparation and their effects on the adsorptive removal of tetracycline is extensively studied. CF derived from zinc nitrate catalyzed agar was studied extensively. Batch adsorption experiments were conducted to assess the effectiveness of CF under varying initial feed concentrations (25-500 mg $L^{-1}$), adsorbent loadings (0.25-1.00 g $L^{-1}$), pH range (4.5-9.8), and temperature range (20-35 °C). A maximum adsorption capacity of 1822 mg $g^{-1}$ was achieved at 500 mg $L^{-1}$ of feed and with an adsorbent loading of 0.25 g $L^{-1}$. The adsorption data were well-described by the Freundlich isotherm, indicating the heterogeneous nature of the CF surface, with multiple adsorption sites resulting in a non-uniform distribution of adsorbate molecules. The adsorption kinetics followed a pseudo-second-order model, suggesting that chemisorption was the

View Article Online
DOI: 10.1039/D5MA00720H

predominant mechanism in the process. Thermodynamic analysis indicated that the adsorption process was endothermic and spontaneous, with a positive entropy change. Additionally, CF demonstrated excellent reusability, maintaining adsorption efficiency over three consecutive cycles.

**Keywords:** Tetracycline, Adsorption, Kinetics, Metal nitrates, Agar, Cellulose

View Article Online
DOI: 10.1039/D5MA00720H



## 1. Introduction:

Water is essential for sustaining life and ensuring a sustainable society. However, rapid industrialization and population growth have led to severe water scarcity and pollution challenges. Among the various pollutants, soluble and insoluble organic compounds are particularly significant [1]. The rising global population, coupled with increased prevalence of viral infections and declining immunity, has led to higher antibiotic usage. This results in elevated levels of antibiotics in wastewater, particularly in developing countries, where monitoring is often inadequate. Additionally, several low and mid-scale industries discharge water without any effective treatment into the river/water bodies despite having stringent laws. Such unregulated pollutant presence can have severe consequences for human health and environmental ecosystems, especially aquatic life [2].

Synthetic pharmaceutical effluents have been extensively studied to remove various pollutants using different techniques in the literature that includes, ion-exchange [3], advanced oxidation processes [4], biological treatment [5], adsorption, and several other integrated approaches. Adsorption is considered one of the most effective techniques for the removal of antibiotics due to its high efficiency, cost-effectiveness, and ease of operation. Several carbon-based materials have been widely investigated for tetracycline removal owing to their large surface area, tunable porosity, and diverse surface functionalities. Foundational work comparing CNTs, activated carbon and graphite established that tetracycline adsorption on graphenic surfaces is driven by π–π electron-donor–acceptor, cation–π and van der Waals interactions, with accessibility of sites strongly affecting affinity[6]. These interactions highlight the potential of defect-rich carbonaceous frameworks in providing abundant active sites for efficient antibiotic removal. Among the several approaches, adsorption technology is widely used and a promising technology due to its cost-

View Article Online
DOI: 10.1039/D5MA00720H



effectiveness, ease of operation, high efficiency, and lack of secondary pollution [7]. However, for commercial scale operations it is important to have a low-cost adsorbent that is abundant in nature that possess a very high adsorption capacity with robust and effective treatment with real industrial effluents. Activated carbons derived from various biomass streams (e.g., coconut shell, walnut shell) are used extensively in industries as an adsorbent but they are found to be expensive and needs to be improved in terms of their adsorption capacity as well as lowering the costs of these adsorbents. In this aspect, a variety of materials have been developed to enhance the adsorption capacity for the removal of antibiotics from wastewater, including carbon-based substances, polymeric materials, clay minerals, metal oxides and metals, and chitosan [8–11]. Carbon based materials are recognized for their effectiveness in removing various pollutants due to their large surface areas, strong interactions with pollutants, and numerous pores. Common carbon materials used for the removal of different pollutants include carbon nanotubes, activated carbon, graphene, CF and their composites [12].

Recent studies have looked into different kinds of 3D porous materials for cleaning up pollutants like antibiotics, dye, oil separation etc. CF is a type of porous carbon material that has a 3D interconnected network structure[13]. CF is a strong, lightweight, sponge-like material with excellent thermal and electrical management capabilities and a large surface area, making it ideal to be used as catalyst supports, filters for molten metals and corrosive chemicals, porous electrodes, and absorbers of impact, energy, and sound [14].

Different type of precursors for CF includes synthetic organic polymers made of petroleum-based materials, such as furfural resin, phenol-formaldehyde, and Poly arylacetylene and it is synthesized by agricultural or waste biomass as precursors such as tannins, fruit waste, and lignocellulosic materials [15–17]. Another good precursor for creating CF is carbohydrates such as agar, sucrose,

View Article Online
DOI: 10.1039/D5MA00720H



starch etc. A common disaccharide with 42.1% carbon content, sucrose readily dehydrates in acidic environments. A macro-porous carbon structure is produced by this method, which may then be further carbonized to make a glassy CF [18,19]. Direct carbonization, hydrothermal treatment, and freeze-drying are just a few of the techniques that have been successfully used to produce CF in which the direct carbonization is the most effective technique [20].

The significance of the present work lies in demonstrating a rapid, low-temperature, and cost-effective strategy for synthesizing ZnO–carbon foam (CF) from a renewable carbohydrate precursor (agar), tailored for the efficient removal of tetracycline as a model antibiotic. Antibiotic contamination is a critical global challenge, not only due to its persistence in aquatic systems but also because of its contribution to antimicrobial resistance. Although a wide variety of biomass-derived carbon materials have been reported for water purification, most existing approaches suffer from inherent drawbacks such as high-temperature carbonization (>500–800 °C), extended processing times, multi-step activation/post-treatments, or reliance on hazardous activating agents, which hinder their scalability and sustainability. To address this research gap, our study introduces a one-step synthesis completed within 10 minutes at only 180 °C, yielding a hierarchical macro–meso–microporous CF structure with in-situ embedded ZnO nanoparticles. This eliminates the need for additional chemical treatments, reduces energy input and cost, and minimizes environmental burden. Beyond establishing an effective proof of concept, this work suggests a sustainable and scalable pathway for developing multifunctional carbonaceous adsorbents that can be extended for the removal of a broader range of emerging organic pollutants from water.

View Article Online
DOI: 10.1039/D5MA00720H



## 2. Experimental

### *2.1. Materials*

All chemicals and reagents used in this study were of analytical grade with high purity (>98%). Agar powder, zinc nitrate hexahydrate ($Zn(NO_3)_2.6H_2O$), ferric nitrate nonahydrate ($Fe(NO_3)_3.9H_2O$), chromium nitrate nonahydrate ($Cr(NO_3)_3.9H_2O$) were purchased from Loba Chemie Pvt. Ltd. Cobalt Nitrate Hexahydrate ($Co(NO_3)_2.6H_2O$) obtained from Fisher Scientific and magnesium nitrate hexahydrate ($Mg(NO_3)_2.6H_2O$), sucrose, starch was received from Merck life science private limited. Cellulose was purchased from Bangalore fine chem. Tetracycline was procured from Cipla Ltd. Distilled water was used for the synthesis of all adsorbents, while reverse osmosis (RO) water was used for the preparation of feed solution.

### *2.2. Synthesis of carbon foam*

The synthesis of CF typically involved mixing of agar and metal nitrate (here: zinc) precursors in different weight ratios (1:2) were mixed in a 100 mL beaker and heated on a hotplate. This mixture was gradually heated and melted into a uniform, thick liquid at a set temperature of 180 °C. As the temperature increases, the solution turns into a yellowish homogenous mixture that eventually converts into a carbonized black foam. Zinc-based CF was synthesized within 10 min through a direct reaction between agar and zinc nitrate. Due to its strong oxidizing properties, metal nitrate precursors in the above mixture break down and interact with the agar powder. Dehydration and polymerization reactions during the pyrolysis of agar will eventually resulting in the formation of a complex foam-like structure that is densely embedded with zinc oxide particles [21].

### *2.3. Experimental procedure*

Tetracycline adsorption studies were carried out in batch mode in which a stock solution of tetracycline (500 mg $L^{-1}$) was initially prepared, and it was further diluted to the desired

View Article Online
DOI: 10.1039/D5MA00720H



concentrations depending on the experiments. Adsorption studies were carried out in conical flasks containing a known amount of CF as an adsorbent and 50 mL of tetracycline solution for a constant time, with different initial concentrations of tetracycline (25 - 500 mg $L^{-1}$), different adsorbent dosages (0.25 - 1 g $L^{-1}$), different pH (4.5 - 9.8) and different temperatures (298, 303, 308 K) in deionized water. Two flasks of identical samples in replicate were placed on magnetic starrier at 250 rpm for 24 h. After the desired time, the mixtures were filtered through a 0.22 μm filter membrane, and the residual tetracycline solutions were analyzed using a UV-visible spectrophotometer (HACH-DR6000) at a maximum absorption wavelength of 358 nm. At equilibrium, the amount of adsorbed $q_e$ (mg $g^{-1}$) pollutant onto the adsorbent was calculated using the following equation (1):

$$q_e = \frac{(C_i - C_e)\,V}{m} \quad (1)$$

Where $C_i$ and $C_e$ are initial and final concentrations of the antibiotic solution (mg $L^{-1}$) at equilibrium state, V and m are the volumes of the antibiotic solution (L) and mass of the adsorbent (g), respectively. Among the non-linear isotherm equations that were used to evaluate the experimental adsorption data were the Langmuir, Freundlich, Temkin models. These equations were used as a means of explaining the characteristics and processes of the adsorption process. The pseudo first order model (PFOM), the pseudo second order model (PSOM), and the intra particle diffusion model (IPDM) were the four kinetic models used to evaluate the adsorption kinetics.

### *2.4. Characterization techniques*

Various techniques were used to characterize all the catalysts synthesized in this study, focusing on their functional groups, crystallinity, surface area analysis. The structural and chemical states of the adsorbent were examined using X-ray powder diffraction (XRD) with a Rigaku Smart Lab

View Article Online
DOI: 10.1039/D5MA00720H



model, scanning in the 2θ range of 10-80° at a speed of 0.1 $s^{-1}$. Additionally, Fourier transform infrared (FTIR) analysis was performed using a Bruker ALPHA instrument, recording spectra in the range of 500 to 4000 $cm^{-1}$. Surface area of the Braunauer Emmett Teller (BET) was measured using a micrometrics Tristar 3000 V6.08 apparatus. A HACH DR6000 UV-Vis spectrophotometer was used to evaluate liquid samples. The morphology was determined, and the elements were subjectively identified using field emission scanning electron microscopy (FESEM; JEOL manufacture JSM-7610 F-Plus equipped with EDX detector).

### *2.5. Statistical analysis*

Initial preliminary studies were carried out more for 5 times to test the reproducibility of the tests which demonstrated >95% confidence level. Based on these initial observations further tests reported in this study were carried out in replicates. More details of the statistical analysis are mentioned in supplementary information.

View Article Online
DOI: 10.1039/D5MA00720H



## 3. Result and discussion

In this section, we discuss the results of CF prepared using different metal precursors, carbon precursors. These different CF were initially tested for adsorption of tetracycline as a model pharmaceutical pollutant. The best performing CF was studied in detail under different operating conditions as follows.

### 3.1. Adsorption studies

#### *3.1.1. Effect of different metal precursors*

Structured carbons or CF were prepared under mild conditions where the organic carbon precursor was catalytically converted in the presence of metal nitrate salts resulting in the formation of ordered structures with high surface areas. Thermal dissociation of these metal nitrates into gases during the process plays a vital role in the foaming process. This study evaluates the role of various catalytic metal precursors such as zinc, cobalt, ferric, chromium, and magnesium in the preparation of CF derived from agar as a carbon precursor in terms of their adsorptive removal of tetracycline. The adsorptive removal of 200 mg $L^{-1}$ of tetracycline studied with 0.25 g $L^{-1}$ under neutral pH conditions is shown in Figure 1. Among the various CF prepared maximum removal efficiencies > ~92% were achieved using cobalt and zinc-based CF. Iron based CF were found to have a removal efficiency up to 78%, whereas magnesium and chromium were found to have relatively lower removal efficiencies of 23 and 35% respectively. These differences in adsorption efficiency are attributed to the distinct structural and chemical characteristics imparted by each metal precursor during the carbonization process. Zinc based CF were studied further in detail owing to their high removal efficiency, low cost and ease of availability, and less toxic, making it more economical for large scale applications. The overall removal efficiency of tetracycline is in the order of Cobalt > Zinc > Iron> Magnesium > Chromium.

View Article Online
DOI: 10.1039/D5MA00720H



Agar, a polysaccharide rich in hydroxyl groups, forms a uniform hydrogel that undergoes gelation and carbonization to produce a stable three-dimensional carbon network. When zinc nitrate is incorporated, the $Zn^{2+}$ ions dissolve completely and distribute evenly within the agar matrix. These ions coordinate with the hydroxyl and glycosidic oxygen atoms of agar, reinforcing the gel network and promoting dehydration and crosslinking at lower temperatures. This accelerates the aromatization of carbon structures, leading to improved structural order. During carbonization, zinc nitrate decomposes to form ZnO nanoparticles and releases gaseous by-products such as $NO_2$ and $O_2$. The evolved gases act as pore-forming agents, creating interconnected macro- and mesopores, while the ZnO particles serve as rigid templates that prevent structural collapse. [22]

$$Zn(NO_3)2.6H_2O + agar \rightarrow C_{Foam} + NOx\uparrow + CO2\uparrow + N2\uparrow + ZnO + H_2O$$

Previous studies in the literature have reported [23] the role of transition metals, such as copper, iron, and nickel, as catalysts in influencing the foaming properties of sugar-based CF. These studies revealed a decrease in micro-pore content with increasing iron concentration after carbonization and activation. Among the metals studied, nickel exhibited the highest foam rise, while iron showed the lowest. Although, the activated CF demonstrated remarkably high surface areas (868 $m^2\ g^{-1}$), their adsorption capacity for methylene blue was relatively low (max 85 mg $g^{-1}$). A magnetic CF derived from phenolic foam catalyzed with iron acetylacetonate was reported [24] to have a surface area of 227.5 $m^2\ g^{-1}$ having an adsorption capacity of 258 mg $g^{-1}$ of Rhodamine-B dye. A hierarchically porous iron containing carbon foam (Fe-CF) synthesized through the carbonization of a nano-magnesium oxide/epoxy resin mixture, followed by activation with ferric nitrate activation was reported to [25] exhibit high adsorption capacities for Congo Red (CR) (1263 mg $g^{-1}$), Malachite Green (MG) (679 mg $g^{-1}$), and Methylene Blue (MB) (484 mg $g^{-1}$).

View Article Online
DOI: 10.1039/D5MA00720H



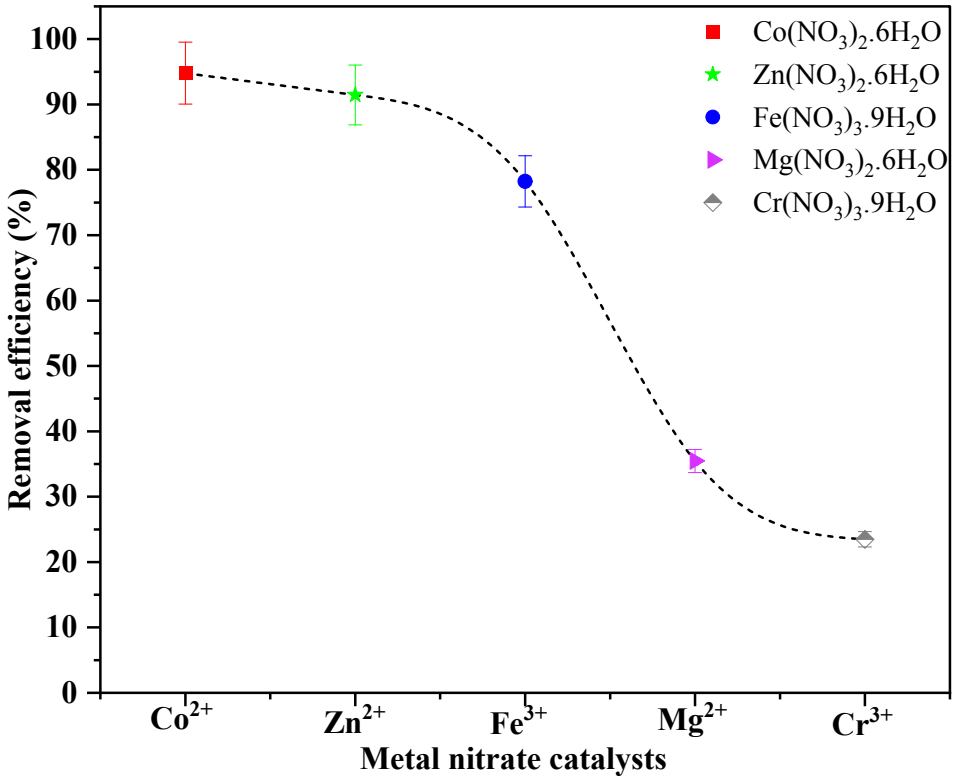


Figure 1: The removal efficiency of tetracycline with Agar based CF catalyzed with different metal nitrates. [Experimental conditions: Feed concentration = 200 mg $L^{-1}$, adsorbent loading = 0.25 g $L^{-1}$, pH =7)

### *3.1.2. Role of different carbon precursors*

Structured CF can be prepared from different carbon precursors such as disaccharides, starch and carboxylic acids, by direct polymerization in the presence of metal catalysts. The foaming reactions are usually exothermic in nature, and they typically occur within the temperature range of 120 – 160 °C leading to a variety of structured CF depending on the carbon precursors used. The purpose of this study is to evaluate the performance of the CF derived from various carbon precursors such as cellulose, sucrose, starch and agar on adsorptive removal of tetracycline as shown in Figure 2. The findings revealed that the CF derived from cellulose exhibited the highest removal efficiency of ~94%, followed by agar at ~93%, sucrose at ~91%, and starch powder at ~90% with 200 mg $L^{-1}$ of tetracycline feed and 0.25 g $L^{-1}$ of adsorbent. These results suggest that

View Article Online
DOI: 10.1039/D5MA00720H



the CF with different precursors have the least impact on the adsorption behavior in terms of tetracycline removal and this can be attributed to the maximum and equivalent amounts of functional groups present in all the CF prepared with different carbon precursors [see section 3.2]. CF derived from different precursors exhibit varying structural properties due to the distinct polymerization reactions that occur with each type of carbon precursor. Polymerization generally proceeds in two steps. The first step involves the evaporation of the solvent (in this case, water), leading to the cleavage of glycosidic bonds between individual monosaccharide units, yielding glucose and fructose [23]. In the second step, the polymerization of hydroxyl (OH) groups occurs, facilitated by catalytic materials. This process forms C-O-C bonds that link the sugar units, constructing the backbone structure of the foam.

Previous reports of CF synthesis from different carbon precursors based on carbohydrates such as glucose, sucrose, starch have been reported [26] to achieve more or less similar adsorption capacities for nickel removal. The adsorption capacities of 48.5, 42.4 and 41.1 mg $g^{-1}$ were obtained with glucose, sucrose and starch derived CF that are activated using phosphoric acid. These CF were having a maximum surface area of 700 $m^2$ $g^{-1}$. CF derived from agar and table salt in 1:4 were reported [27] to have a surface area of 365 $m^2$ $g^{-1}$ and they exhibited a high oil/organic solvent adsorption capacity ranging from 84 – 202 times its own weight. While CF prepared using zinc nitrate catalyst with different carbohydrates such as glucose, maltose, and starch were reported [28] to have similar adsorption capacities of 376, 378, 377 mg $g^{-1}$ for tetracycline removal. The surface areas of these CF were found to be 48.9, 40.9 and 38.1 $m^2$ $g^{-1}$ with glucose, maltose and sucrose respectively. Similar observations were made when CF prepared from sucrose and zinc nitrate hexahydrate (1:2) which demonstrated a removal efficiency of 77% for malachite green [29]. Therefore, CF derived from various carbon precursors exhibited comparable adsorption capacities

View Article Online
DOI: 10.1039/D5MA00720H



for pollutants, owing to their similar functional group content and structural properties influenced by precursor-specific polymerization reactions.

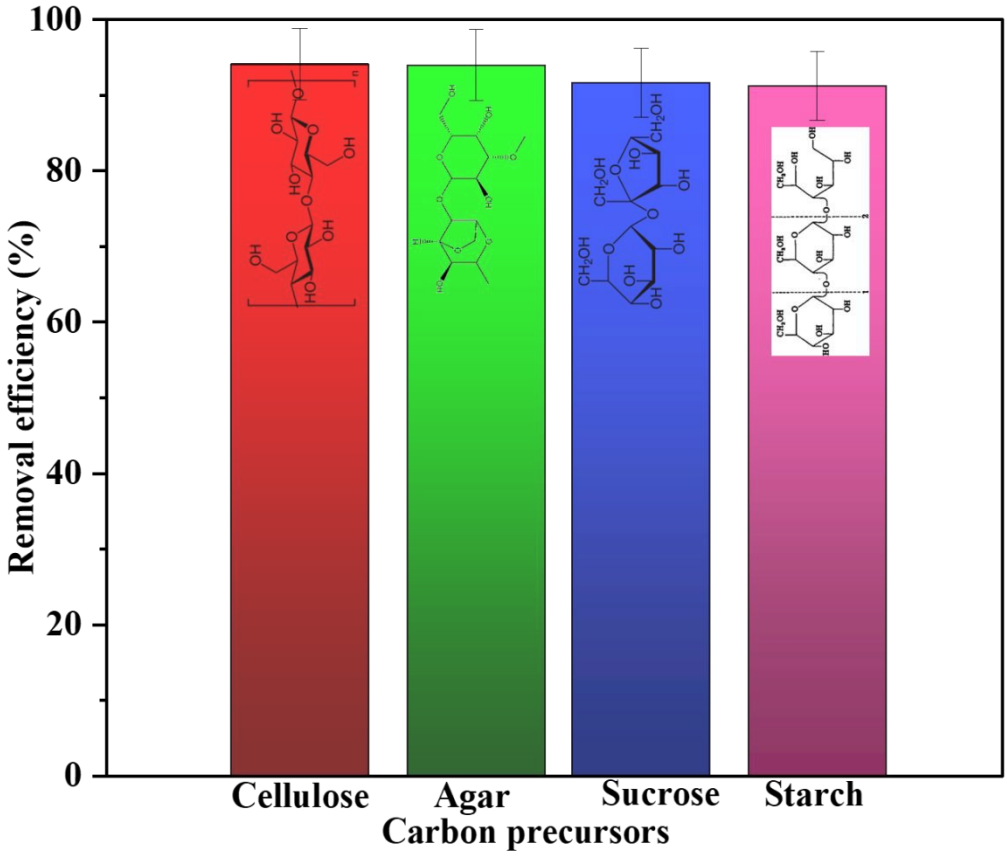


Figure 2: Influence of different CF derived from various carbon-based precursors catalyzed with zinc nitrate on the removal efficiency of tetracycline. [Experimental conditions: Feed concentration = 200 mg $L^{-1}$, adsorbent loading = 0.25 g $L^{-1}$, pH = 7]

### *3.1.3. Adsorption of different antibiotics:*

Based on the above screening studies, further detailed studies were conducted with agar based CF prepared in the presence of zinc nitrate catalyst. Preliminary studies were focused in evaluating the performance of the CF in the removal efficiency of various synthetic pharmaceutical model compounds. The adsorption studies with CF derived from agar catalyzed by zinc catalyst is studied for the removal of different antibiotics such as ciprofloxacin, tetracycline, azithromycin, and

View Article Online
DOI: 10.1039/D5MA00720H



amoxicillin and the results are presented in Figure 3. The results indicate that the removal efficiencies for tetracycline and ciprofloxacin are notably high, at ~87% and ~78%, respectively. In contrast, the removal efficiency for amoxicillin and azithromycin are considerably lower, at 39% and 29%, respectively. These notable changes in the removal efficiency highlight the selective adsorption capability of CF towards different antibiotics, likely attributable to the pollutant's molecular structure, interactions with the CF's porous network and surface functionality.

Tetracycline and ciprofloxacin possess relatively compact molecular structures with multiple functional groups, such as hydroxyl, amine, and carboxyl groups, capable of forming hydrogen bonds with the zinc-catalyzed CF surface. The presence of oxygenated functional groups (e.g., C=O, -OH) on the CF, along with residual zinc species, facilitates hydrogen bonding and electrostatic interactions with these antibiotics. Additionally, the pore size of the CF is an important parameter, likely aligning well with the smaller molecular dimensions of tetracycline and ciprofloxacin, enabling their efficient diffusion into the porous structure. In contrast, azithromycin, with its bulky macrolide structure, and amoxicillin, with a larger amine side chain, face steric hindrance that impedes their diffusion into the CF's micropores. These synergistic factors collectively account for the higher adsorption efficiencies observed for tetracycline and ciprofloxacin compared to the bulkier molecules, such as azithromycin and amoxicillin. These structure-dependent differences are consistent with the overall adsorption mechanism proposed in this study. While smaller, planar antibiotics (tetracycline and ciprofloxacin) can exploit hydrogen bonding, electrostatic interactions, and π–π stacking with the CF surface, bulkier molecules such as azithromycin and amoxicillin are sterically hindered from accessing micropores and forming such interactions. This highlights that the selective adsorption capability of CF arises from the

View Article Online
DOI: 10.1039/D5MA00720H



interplay between its hierarchical porous structure, surface functionality, and the molecular architecture of the pollutants.

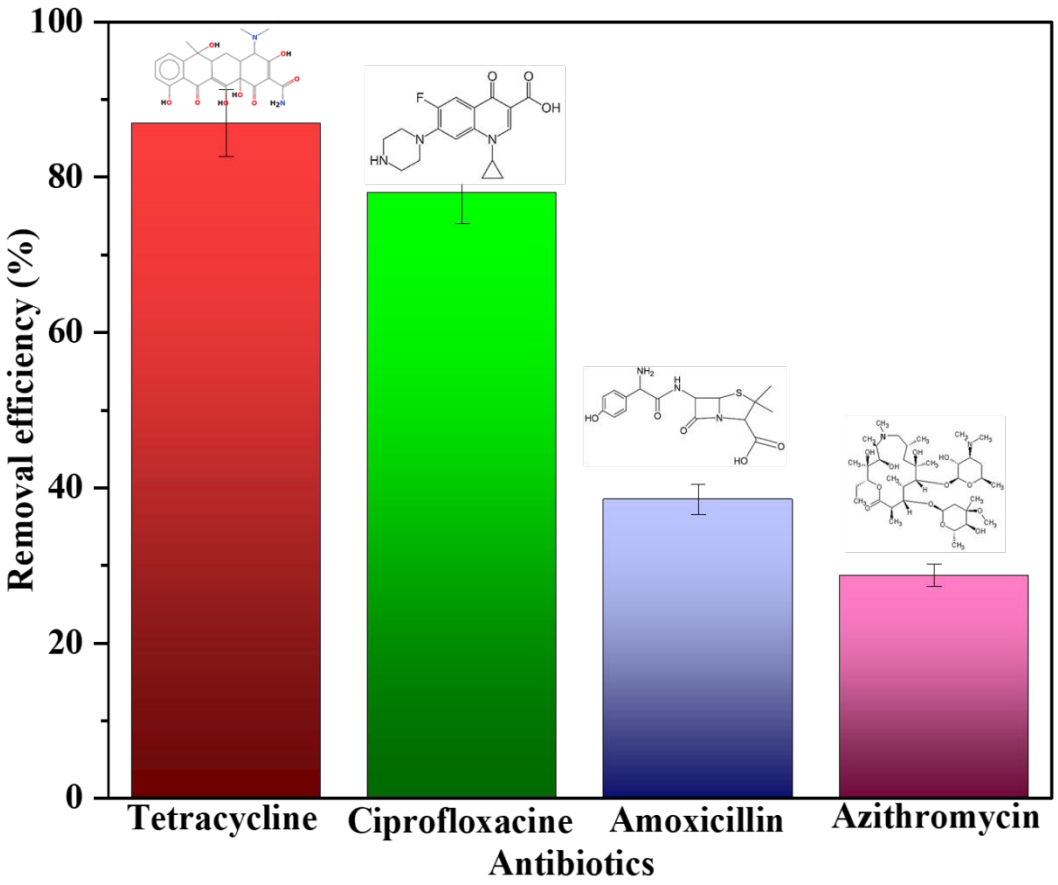


Figure 3: Removal efficiency of different antibiotics with zinc catalyzed agar derived CF. [Experimental conditions: Feed concentration = 50 mg $L^{-1}$, absorbent loading = 1 g $L^{-1}$, Temperature = 30 °C, pH = 7]

### *3.1.4. Effect of adsorbent loading:*

The influence of different adsorbent loadings ranging from 0.25 to 1 g $L^{-1}$ on the removal efficiencies of tetracycline is shown in Figure 4. It is evident from the figure that the removal efficiency reduced slightly from 92 to 89% with decreasing the adsorbent dosage from 1 to 0.25 g $L^{-1}$. It is noteworthy that the adsorbent capacity increases by four folds from 174 mg $g^{-1}$ to 724 mg

View Article Online
DOI: 10.1039/D5MA00720H



$g^{-1}$ with a drop in adsorbent loading from 1 to 0.25 g $L^{-1}$. This trend suggests that, at lower dosages, the adsorbent's ultra-high capacity enables more efficient utilization of its active sites, leading to a higher adsorption capacity per unit mass. At higher dosages, the number of available active sites exceeds, leading to underutilization of the adsorbent and a reduction in the specific adsorption capacity. Nevertheless, the overall removal efficiency remains high due to the increased mass of adsorbent in the system. Indeed, similar adsorption characteristics were reported [21] in the elsewhere with adsorbents possessing super adsorption capacities under different adsorbent loadings.

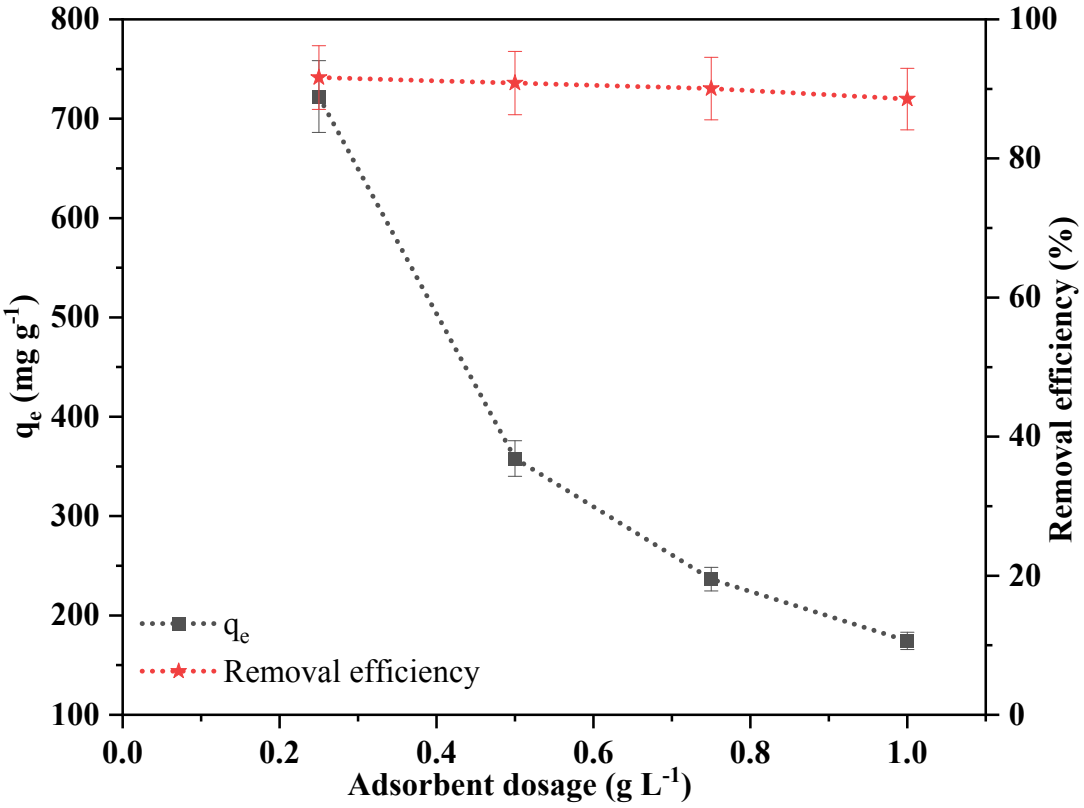


Figure 4: Effect of adsorbent loading on the adsorption capacity of CF and the removal efficiency of tetracycline. [Experimental conditions: Feed concentration = 200 mg $L^{-1}$, adsorbent loading = 0.25 to 1 g $L^{-1}$, pH = 7].

### *3.1.5. Effect of feed concentration:*

View Article Online
DOI: 10.1039/D5MA00720H



The impact of feed concentration on the adsorption of tetracycline was studied within the range of 25 – 500 mg $L^{-1}$ at a constant adsorbent dosage 0.25 g $L^{-1}$ and the results are shown in Figure 5. As the initial concentration increased from 25 to 500 mg $L^{-1}$, the adsorption capacity rose significantly from 48 to 1822 mg $g^{-1}$. The notable increase in adsorption capacity with higher initial feed concentrations can be attributed to the increased concentration gradient, which provides a stronger driving force for adsorption. At elevated concentrations, there is a greater availability of tetracycline molecules, which increases the likelihood of adsorption onto the available active sites of the adsorbent. This enhanced interaction results in a more effective utilization of the adsorbent's capacity until equilibrium is reached. As a result, the equilibrium adsorption capacity significantly increases as the feed concentration rises [30].

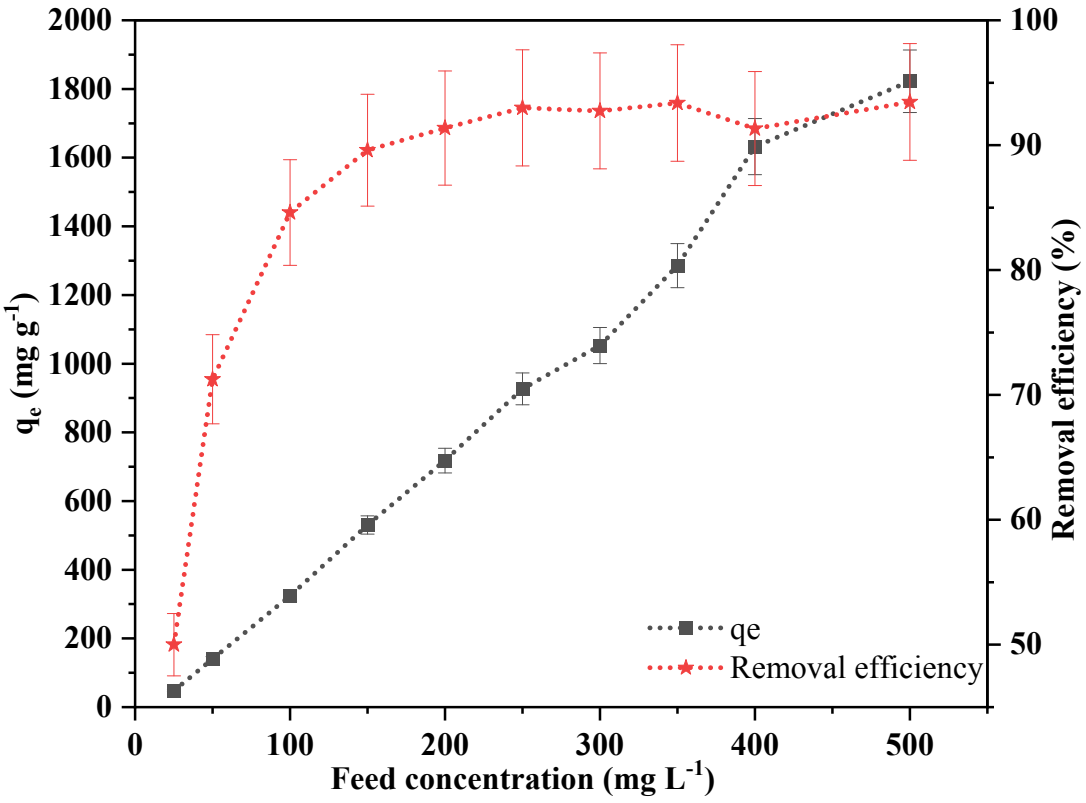

View Article Online
DOI: 10.1039/D5MA00720H

Figure 5: Effect of initial feed concentration of tetracycline on the equilibrium adsorption capacity and removal efficiency with CF. [Experimental conditions: Feed concentration = 25 to 500 mg $L^{-1}$, adsorbent loading = 0.25 g $L^{-1}$, pH = 7).

### *3.1.6. Effect of contact time:*

The equilibrium adsorption capacity was determined by studying the variation in the adsorption capacity with time over a 24 h period with three different feed concentrations of tetracycline (100, 200 and 500 mg $L^{-1}$). Both removal efficiency and the adsorption capacity increased with increasing contact time until the equilibrium was reached (Figure 6). Initially, a sharp increase in adsorption capacity was observed, which can be attributed to the rapid occupation of available adsorption sites on the adsorbent, facilitated by the high availability of unoccupied sites during the early stages. The results indicate that equilibrium for tetracycline adsorption was achieved within 3 h. These observations are reported [31] in the literature where the equilibrium adsorption capacity depends on the type of pollutant, adsorbent, and initial feed concentration.

View Article Online
DOI: 10.1039/D5MA00720H



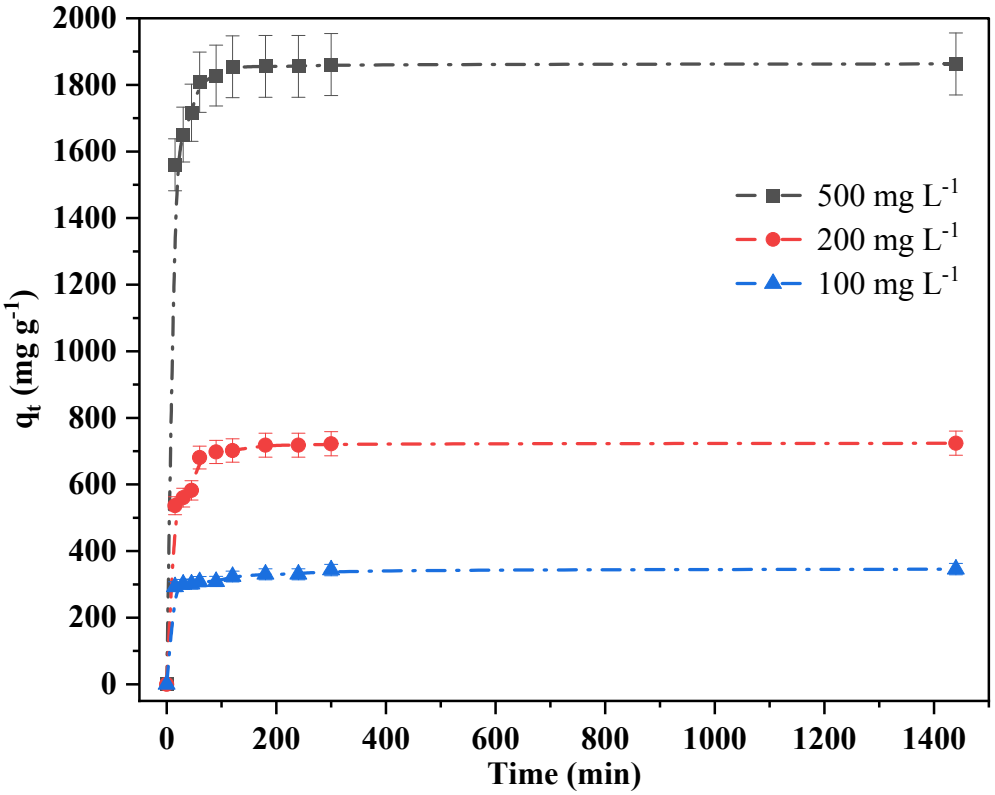


Figure 6: Effect of contact time on the adsorption capacity of tetracycline over CF. [Experimental conditions: Feed concentration = 100, 200, 500 mg $L^{-1}$, adsorbent loading = 0.25 g $L^{-1}$, pH = 7)

### *3.1.7. Effect of pH*

The initial pH of the solution is a critical parameter influencing the adsorption process, as it affects both the surface charge of the adsorbent and the ionization state of the adsorbate, thereby impacting interaction mechanisms and overall efficiency. The pH effect on tetracycline adsorption was studied by adjusting the solution pH from 4.5 to 9.8 with 0.25 g $L^{-1}$ of adsorbent. The pH range of 4.5–9.8 was selected as it encompasses slightly acidic, neutral, and basic conditions commonly encountered in natural waters and wastewater effluents (typically pH 6–9). This range allows evaluation of adsorption behavior across environmentally relevant conditions, ensuring practical significance for real water treatment applications. As shown in Figure 7a, the adsorption capacity increased from 664 mg $g^{-1}$ at pH 4.5 to 725 mg $g^{-1}$ at pH 7 and reached ~731 mg $g^{-1}$ at pH 9.8. At

View Article Online
DOI: 10.1039/D5MA00720H



higher pH, both the carbon foam surface and tetracycline molecules become negatively charged, which typically leads to electrostatic repulsion. However, strong surface complexation/chemisorption and π–π interactions can overcome these barriers, enabling selective uptake even under unfavorable conditions[32,33]. The presence of abundant surface defects and functional groups further provides additional binding sites, contributing to the high adsorption efficiency. Conversely, at acidic pH, the removal efficiency slightly decreased due to increased protonation of active sites and electrostatic repulsion, though hydrogen bonding and π–π interactions still facilitated adsorption. These results highlight the significant role of pH in controlling tetracycline uptake by carbon foam, with neutral to alkaline conditions being optimal. A similar trend was reported [34,35] in another study, where the adsorption capacity increased from 76.3 to 215 mg $g^{-1}$ as the pH rose from 2 to 7 and remained around 205 mg $g^{-1}$ at pH 10. At lower pH, increased protonation of active sites led to enhanced electrostatic repulsion, thereby decreasing adsorption efficiency.

The zeta potential data for CF across different pH values provides insight into their surface charge and interaction with tetracycline pollutant (Figure 7b). The CF show a point of zero charge (PZC) around pH 7, indicating minimal surface charge at neutral pH. At acidic pH (3.5 to 7), the CF surface is slightly negative, while tetracycline exists in its cationic form. This creates favorable conditions for electrostatic attraction, particularly at lower pH levels like 3.5, where the negative surface charge of the CF supports adsorption. As pH increases, the zeta potential becomes more negative where CF are highly negatively charged at pH 8.5. However, at this pH, tetracycline begins to transition into its anionic form, leading to electrostatic repulsion and a decrease in adsorption. At highly alkaline pH (11.5), both the CF surface and tetracycline are negatively charged, further inhibiting adsorption due to repulsive forces.

View Article Online
DOI: 10.1039/D5MA00720H



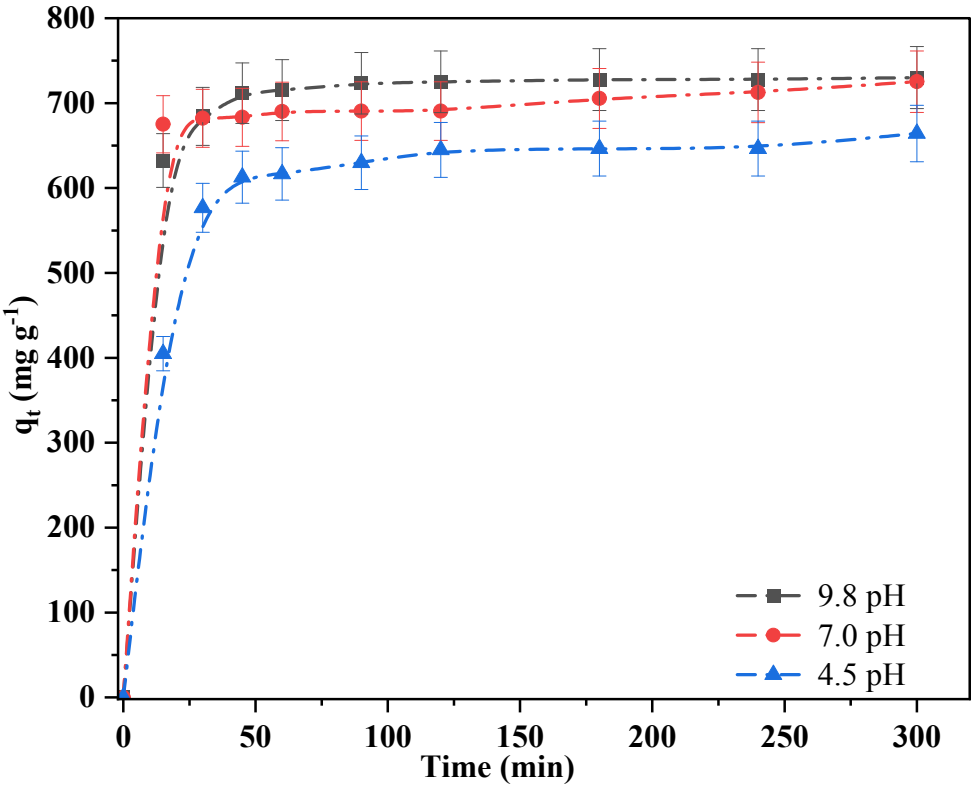


366

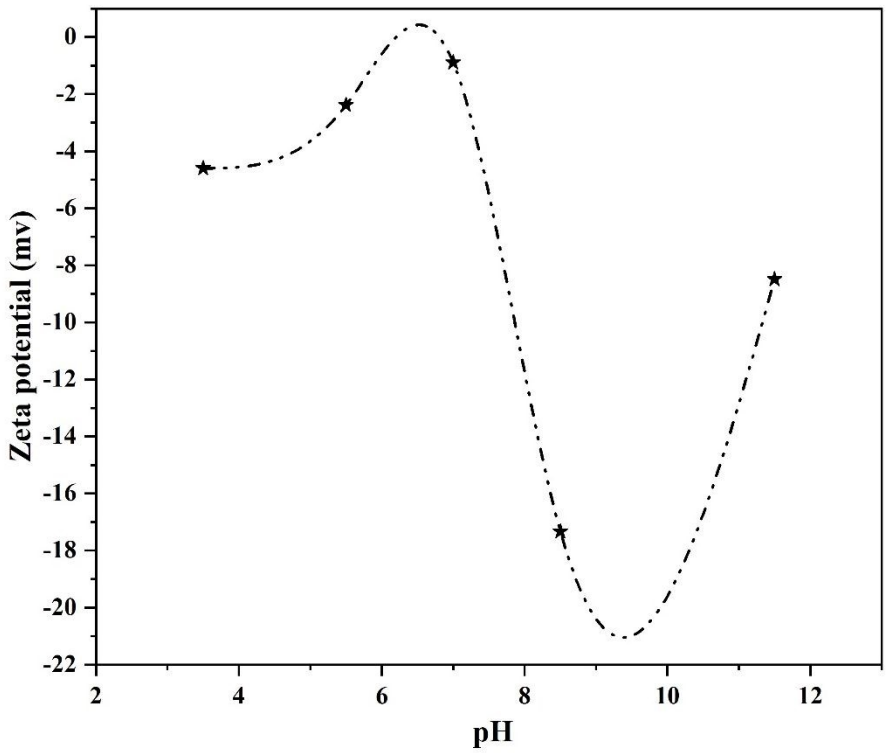


367

View Article Online
DOI: 10.1039/D5MA00720H

Figure 7: Effect of different solution pH on a) the adsorption capacity of tetracycline over CF and b) Zetapotential values of CF. (Experimental conditions: Feed concentration = 200 mg $L^{-1}$, adsorbent loading = 0.25 g $L^{-1}$).

### *3.1.8. Effect of temperature:*

To understand the adsorption behavior of CF towards tetracycline, adsorption capacity was studied over a temperature range of 293–308 K at different initial concentrations of tetracycline (50, 100, and 200 mg $L^{-1}$). The tested temperatures (20–35 °C) were chosen to reflect realistic environmental and operational conditions in aquatic systems and wastewater treatment processes. This range covers typical seasonal and climatic variations, from temperate regions (~20 °C) to tropical/subtropical conditions (~35 °C), thereby ensuring the relevance of the adsorption results to actual field applications. Adsorption studies at a range of temperatures is crucial for determining the thermodynamic feasibility and understanding the nature of interactions between the adsorbent and the adsorbate. It provides insights into the endothermic or exothermic nature of the adsorption process and reveals how temperature influences the spontaneity and mechanism of adsorption that is essential for designing efficient adsorption systems. Thermodynamic analysis was conducted to determine the mechanism of adsorption by calculating key thermodynamic parameters, including Gibbs free energy (ΔG), enthalpy change (ΔH), and entropy change (ΔS).

The change in Gibbs free energy (ΔG) was calculated using Eq. 3, while the adsorption entropy (ΔS) and adsorption enthalpy (ΔH) were calculated from the slope and intercept of the plot of ln K versus 1/T. A comprehensive summary of all calculated thermodynamic properties is provided in Table 1.

$$K = \frac{q_e}{C_e} \quad (2)$$

$$\Delta G = -RTln(K) \quad (3)$$

$$ln(K) = \frac{\Delta S}{R} - \frac{\Delta H}{RT} \quad (4)$$

View Article Online
DOI: 10.1039/D5MA00720H



where T is the temperature in kelvin, R is the gas constant (8.314 J $mol^{-1}$ $K^{-1}$). ΔG, ΔH, and ΔS are the Gibbs free energy (kJ $mol^{-1}$), enthalpy (kJ·$mol^{-1}$), entropy (kJ $mol^{-1}$ $K^{-1}$). K represents the equilibrium constant, determined by the ratio of $q_e$ (adsorption capacity in mg $g^{-1}$) to $C_e$ (equilibrium concentration in mg $L^{-1}$) [36].

Table 1: Thermodynamic analysis of tetracycline adsorption on carbon foam.

| $C_o$ (mg. $L^{-1}$) | ΔH° (kJ $mol^{-1}$) | ΔS° (kJ $mol^{-1}$ $K^{-1}$) | ΔG° (kJ $mol^{-1}$) | | |
|---|---|---|---|---|---|
| | | | 20 °C | 30 °C | 35 °C |
| 50 | 6.206 | 0.0397 | -5.255 | -5.759 | -6.078 |
| 100 | 2.856 | 0.0358 | -7.660 | -7.934 | -8.221 |
| 200 | 9.799 | 0.0645 | -9.071 | -9.808 | -10.038 |

The negative values of ΔG for the adsorption of tetracycline onto CF indicate that the adsorption process is thermodynamically favorable and spontaneous across the studied temperature range. As the temperature increases, ΔG becomes more negative, suggesting that higher temperatures enhance the adsorption of tetracycline. The calculated ΔG values ranged from -20 to 0 kJ $mol^{-1}$, suggesting that physical adsorption is the predominant mechanism [37].

The positive ΔH value indicates that the adsorption process is endothermic, meaning higher temperatures favor greater adsorption of tetracycline. The relatively low ΔH value (less than 40 kJ $mol^{-1}$) is consistent with physisorption as the dominant mechanism [7]. This behavior confirms that the adsorption process is enhanced with increasing temperature. Additionally, the positive ΔS value suggests an increase in randomness at the solid-solution interface during adsorption, likely due to the displacement of structured water molecules or ions. This entropy increase contributes to the favorability of the adsorption process when accompanied by a sufficiently negative ΔH to ensure an overall negative ΔG. The positive ΔS also implies the stability and irreversibility of the adsorption process[38].

View Article Online
DOI: 10.1039/D5MA00720H



### *3.1.9. Adsorption kinetics*

The kinetics of tetracycline adsorption on to CF plays a vital role to gain insights into the adsorption mechanism and understand the effect of contact time on the adsorption capacity. The kinetic data was obtained by recording tetracycline concentration at fixed time intervals with varied initial feed concentrations and was modeled using the pseudo-first-order, pseudo-second order and intra-particle diffusion model equations as shown in Eq. (5) to Eq (7) respectively.

The pseudo-first order kinetic model (PFOM):

$$\ln(q_e - q_t) = ln(q_e) - k_1 t \quad (5)$$

where $k_1$ is the pseudo first-order adsorption rate constant ($min^{-1}$), $q_t$ is adsorption capacity (mg $g^{-1}$) at time ($t$) and $q_e$ is the adsorption capacity at equilibrium (mg $g^{-1}$).

The pseudo-second-order kinetic model (PSOM):

$$\frac{t}{q_t} = \frac{1}{k_2\, q_e^2} + \frac{1}{q_e}(t) \quad (6)$$

Where $q_e$ is adsorption capacity (mg $g^{-1}$) at equilibrium and $k_2$ is the equilibrium rate constant ($min^{-1}$) for second-order kinetics.

The intraparticle diffusion model (IPDM), introduced by Weber and Morris [39].

$$q_t = k_i\, t^{1/2} + C \quad (7)$$

Where $q_t$ is the adsorption capacity (mg $g^{-1}$) at the time, $t$ (min). $k_i$ (mg $g^{-1}$ $h^{-1/2}$) is the intraparticle diffusion rate constant and $C$ is associated to the boundary layer thickness.

Table 2: Kinetic model parameters of adsorption of Tetracycline on carbon foam

| **Concentration (mg $L^{-1}$)** | **$q_{cal}$ (mg $g^{-1}$)** | **PFOM** | **PSOM** | **IPDM** |
|---|---|---|---|---|
| 100 | 340 | $K_1$ = 0.007 ($min^{-1}$) | $K_2$ = 0.0005 (g $mg^{-1}$ $min^{-1}$) | $K_{i-1}$ =2.866, $K_{i-2}$ = 0.474 (mg $g^{-1}$ $min^{-0.5}$) |

View Article Online
DOI: 10.1039/D5MA00720H



| | | | | |
|---|---|---|---|---|
| | | $q_e$ = 280 (mg $g^{-1}$) | $q_e$ =345 | $C_1$ =283.1 (mg $g^{-1}$)<br>$C_2$ =323.6 (mg $g^{-1}$) |
| | | $R^2$ = 0.9597 | $R^2$ =0.999 | $R_1^2$=0.909<br>$R_2^2$ = 0.797 |
| 200 | 724 | $K_1$ =0.0156 ($min^{-1}$)<br>$q_e$ = 340 (mg $g^{-1}$)<br>$R^2$ = 0.9442 | $K_2$ = 0.003 (g $mg^{-1}$ $min^{-1}$)<br>$q_e$ = 720 (g $mg^{-1}$ $min^{-1}$)<br>$R^2$ = 0.999 | $K_{i-1}$=32.09,<br>$K_{i-2}$ = 0.596 (mg $g^{-1}$ $min^{-0.5}$)<br>$C_1$=397,<br>$C_2$ = 703 (mg $g^{-1}$)<br>$R_1^2$ = 0.881,<br>$R_2^2$= 0.503 |
| 500 | 1822 | $K_1$ = 0.0181 ($min^{-1}$)<br>$q_e$ = 960 (mg $g^{-1}$)<br>$R^2$ = 0.9543 | $K_2$ = 0.0002 (g $mg^{-1}$ $min^{-1}$)<br>$q_e$ = 1922 (g $mg^{-1}$ $min^{-1}$)<br>$R^2$ =0.999 | $K_{i-1}$ = 50.65,<br>$K_{i-2}$ = 0.491 (mg $g^{-1}$ $min^{-0.5}$)<br>$C_1$=1339,<br>$C_2$=1809 (mg $g^{-1}$)<br>$R_1^2$=0.9505<br>$R_2^2$=0.609 |

The results of the model fitting for the adsorption kinetics are illustrated in Figure 8, and the corresponding kinetic parameters are presented in Table 2. In comparison to the PFOM with $R^2$ value of 0.9443–0.9597, the PSOM illustrated a better fit to describe the adsorption process of tetracycline over the CF. Additionally, the fitted kinetic parameter values for adsorption capacity ($q_e$) determined from PFOM differed from the experimental values ($q_{cal}$) at equilibrium [40]. The high $R^2$ values of 0.99-1.00 for PSOM reflects that this model effectively describes the adsorption kinetics at varied feed concentrations. The $q_e$ values determined using PSOM fitting agrees well with the experimental values for various feed concentrations (100, 200, 500 mg $L^{-1}$) in this study. This indicates that the adsorption process is primarily driven by chemisorption of tetracycline onto the CF, where the rate of adsorption is dependent on the availability of active sites on the solid surface [40,41]. Further, the mass transfer resistances in the adsorption process were evaluated by

View Article Online
DOI: 10.1039/D5MA00720H



443 modelling the kinetic data using IPD kinetic model. According to this model, the adsorption
444 process is solely controlled by intra-particle diffusion if the data forms a straight line through the
445 origin, implying a *C* value of zero. However, the process may involve multiple phases if the fit
446 requires several linear segments [42]. Figure 8 showed that the adsorption process occurs in two
447 distinct steps. The initial rapid adsorption in the first step is attributed to the diffusion on the
448 external surface due to the boundary layer, followed by a slower rate in the second stage,
449 representing intra-particle diffusion of tetracycline.

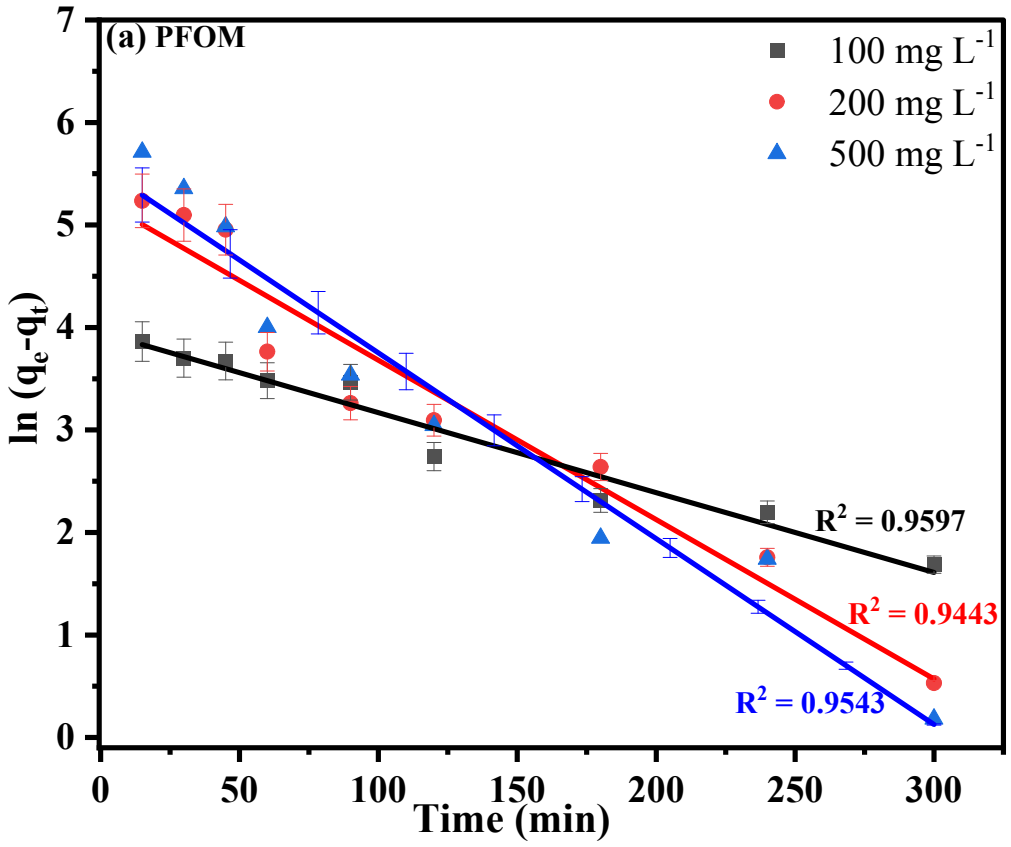


450

View Article Online
DOI: 10.1039/D5MA00720H



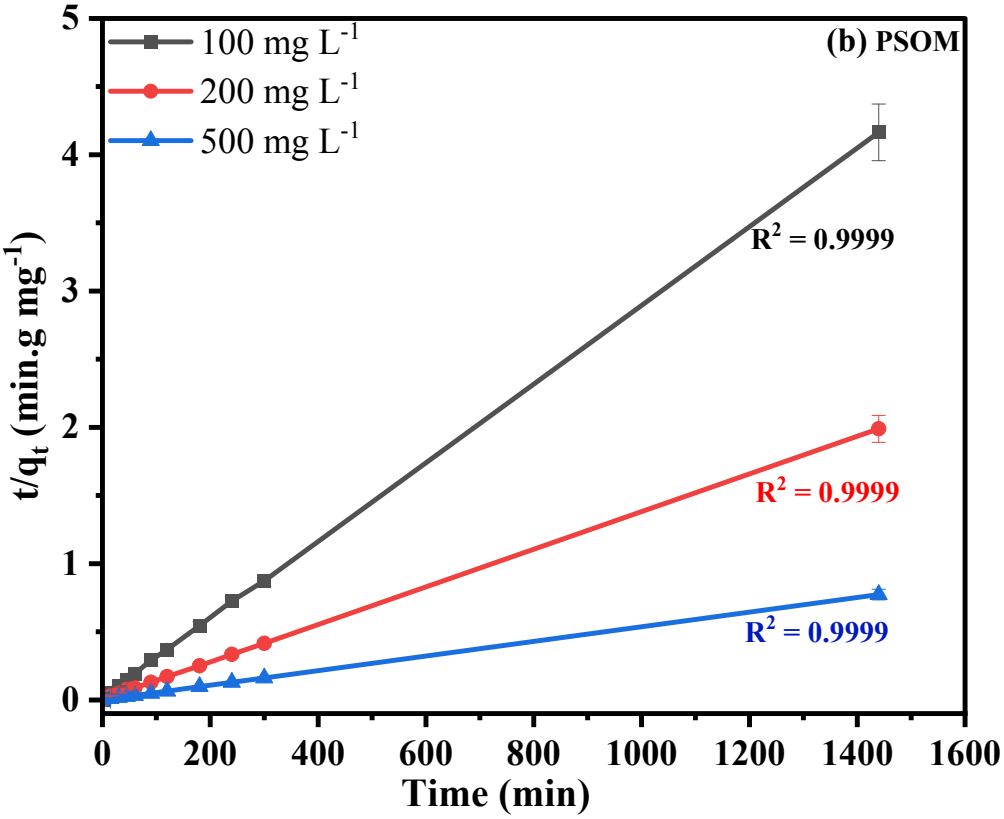


451

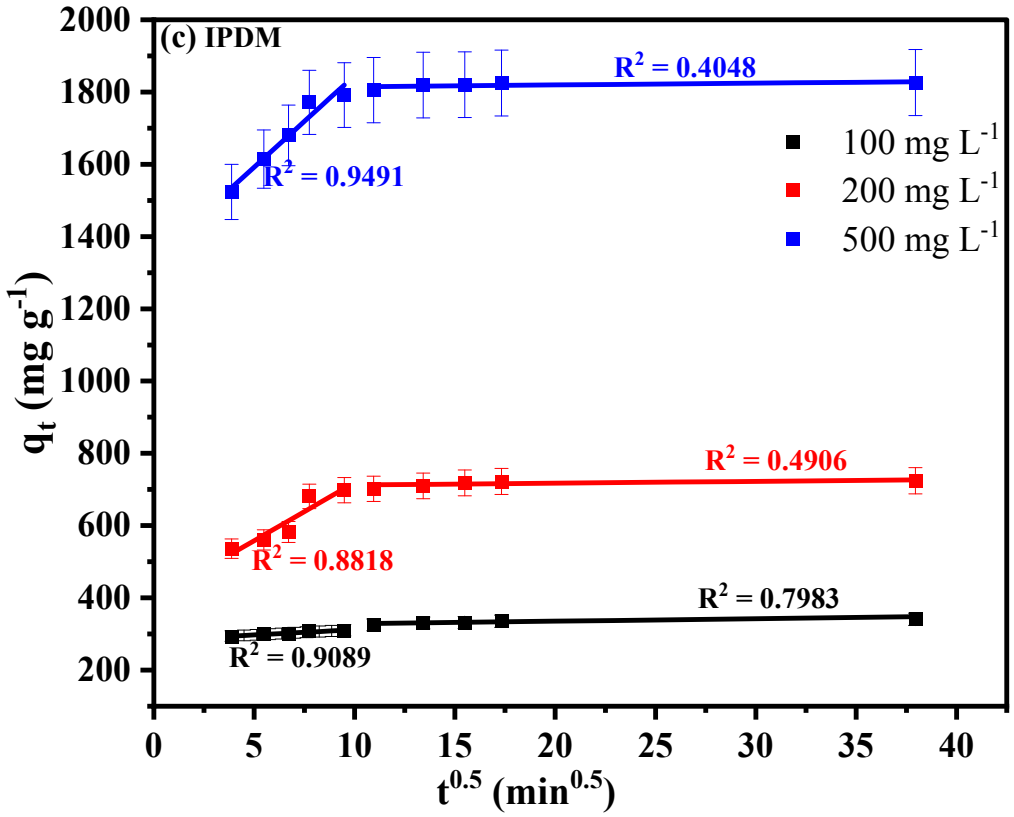


452

View Article Online
DOI: 10.1039/D5MA00720H

Figure 8: Kinetic modelling studies for the adsorption of tetracycline over CF using (a) pseudo first-order (b) pseudo second order (c) IPDM.

The PSOM model appears to have the best fit across all the concentrations, with $R^2$ values close to 1, indicating that the adsorption kinetics followed a pseudo-second-order process. Although the PFOM model provides a reasonable fit, it is less accurate than the PSOM. The IPDM model further indicates presence of multiple stages in the adsorption process, as evidenced by the different slopes in the plots. A pseudo-second order adsorption kinetics mechanism was reported [24] to be a better fit to describe the Rhodamine-B dye adsorption on a phenolic foam-derived magnetic CF with a adsorption capacity of 258 mg $g^{-1}$. Similarly, pseudo-second order was shown to be a best fit for various dyes (Crystal violet, Malachite green and Congo red) adsorption on to starch derived zinc based CF that was reported [30] to exhibit ultra-high adsorption capacity towards Crystal Violet (25000 mg $g^{-1}$), Malachite Green (1200 mg $g^{-1}$) & Congo Red (1429 mg $g^{-1}$).

### *3.1.10. Adsorption isotherms*

Adsorption isotherms are crucial for understanding the distribution of molecules (adsorbate) between a liquid phase and a solid surface (adsorbent) at equilibrium. This study evaluates the applicability of three classical adsorption models: the Langmuir, Freundlich, and Temkin models in characterizing the adsorption of tetracycline on CF. The results of the adsorption isotherm fittings and the estimated model parameters are presented in Figure 9 and Table 3. The Langmuir, Freundlich, and Temkin model equations are given below in Eq (8), Eq (9) and Eq (10) respectively.

$$\frac{1}{q_e} = \frac{1}{q_m} + \frac{1}{q_e K_L C_e} \quad (8)$$

$$\ln(q_e) = ln(K_f) + \frac{1}{n} ln(C_e) \quad (9)$$

$$q_e = Bln(K_t) + Bln(C_e) \quad (10)$$

View Article Online
DOI: 10.1039/D5MA00720H



476 where $C_e$ is the equilibrium concentration (mg $L^{-1}$), $q_m$ is maximum adsorption capacity (mg $g^{-1}$),
477 $q_e$ is the adsorption capacity (mg $g^{-1}$) at equilibrium and $K_L$ is the Langmuir adsorption rate
478 constant. $K_f$ and n are Freundlich constants, where $K_f$ is related to the adsorption capacity, and 1/n
479 indicates the adsorption intensity. B is a constant related to the heat of adsorption, which can be
480 calculated as: $B = RT/b_T$, R is the universal gas constant (8.314 J $mol^{-1} \cdot K^{-1}$) and T is the absolute
481 temperature in Kelvin (K). $b_T$ is the Temkin constant related to the heat of adsorption (J $mol^{-1}$) [41].

482 Table 3: Isotherm's equations and constants for tetracycline adsorption on carbon foam:

| **Isotherms** | **Parameters** | **Values** |
|---|---|---|
| Langmuir | $q_m$ (mg $g^{-1}$) | 1756 |
| | $K_L$ (L $mg^{-1}$) | 7.47 |
| | $R^2$ | 0.966 |
| Freundlich | $K_F$ (mg $g^{-1}$) (L $mg^{-1})^{1/n}$ | 1831 |
| | n | 4.5 |
| | $R^2$ | 0.98 |
| Temkin | $K_R$ (L. $g^{-1}$) | 0.086 |
| | $b_T$ (J $mol^{-1}$) | 1.26 |
| | $R^2$ | 0.946 |

483

View Article Online
DOI: 10.1039/D5MA00720H



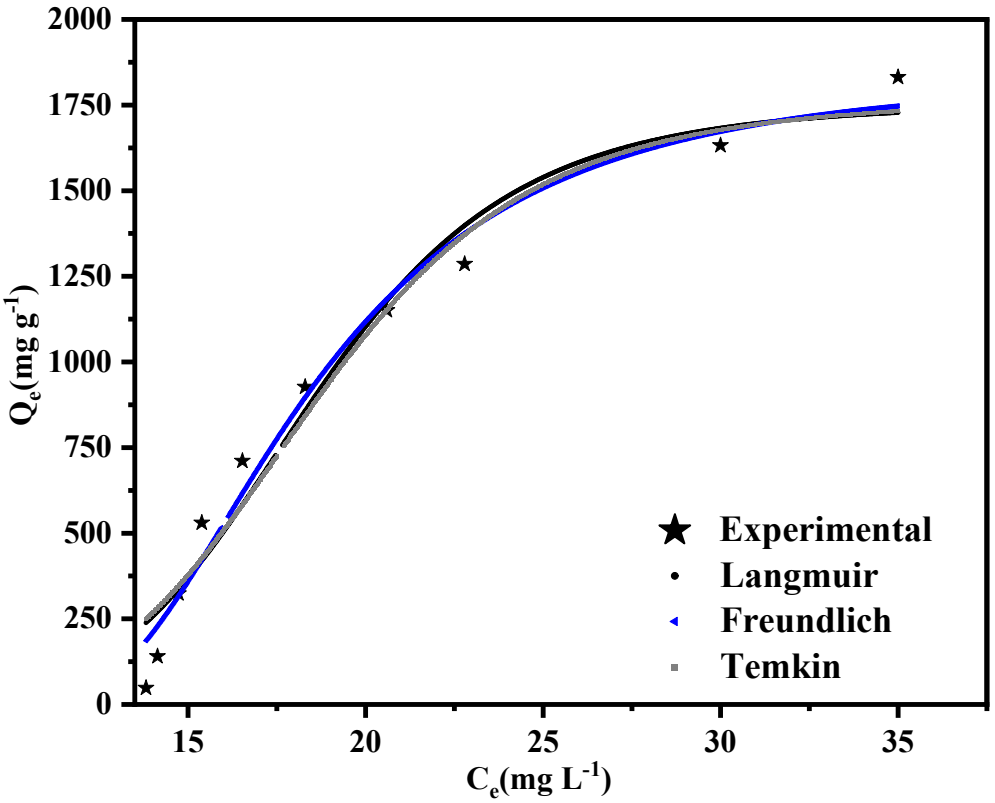


Figure 9: Adsorption isotherm fitting for tetracycline removal over CF.

The Langmuir model is regarded as an ideal representation of adsorption, as it assumes a uniform adsorbent surface and that adsorbate molecules form a monolayer without interacting with one another. In this study, the model yielded an $R^2$ value of 0.966. Notably, the experimental maximal adsorption capacity exceeds the $q_m$ value predicted by the Langmuir model. This discrepancy indicates that the Langmuir model underestimates the actual adsorption capability of the adsorbent[43]. The Freundlich isotherm accounts for non-ideal adsorption behavior, allowing the multilayer adsorption on the surface. This model is particularly useful for describing heterogeneous systems characterized by varying energy sites and differing adsorption strengths. In this study, the Freundlich model demonstrated a high $R^2$ value of 0.980, indicating an excellent fit to the experimental data. The calculated $n^{-1}$ value of 0.22 suggests that the adsorption process is favored and reflects the heterogeneous nature of the adsorbent surface, where variations in site

View Article Online
DOI: 10.1039/D5MA00720H



energies significantly influence overall adsorption behavior[44]. Our results were found to be in line with the literature studies that used corn straw based porous carbon for tetracycline adsorption[45]. The Temkin isotherm model is particularly effective for describing chemical adsorption processes, especially in cases where there is a significant electrostatic attraction between oppositely charged species. This model accounts for the interaction of energy between adsorbed molecules, which can influence the adsorption process. In this study, the Temkin model provided a reasonable fit, with an $R^2$ value of 0.947. A key parameter in the Temkin isotherm, the constant $b_T$, reflects the variation in adsorption energy as the process progresses. This constant is instrumental in understanding the thermodynamic nature of adsorption, specifically indicating whether the process is exothermic or endothermic. If $b_T$ value falls within a range of 1-10, the adsorption is generally considered exothermic, while $b_T$ value close to 0 indicates an endothermic process. In this study, the obtained $b_T$ value of 1.26, being close to 1, signifies a mildly exothermic process with moderate energy release, reflecting favorable adsorbent-adsorbate interactions[39,46].

The comparison in Table 4 highlights the remarkable performance of carbon-based adsorbents for the removal of tetracycline, with a clear ranking of adsorption capacities ($q_e$). The CF derived from agar in this study shows the highest adsorption capacity at 1831 mg $g^{-1}$, outperforming a variety of other carbon-based materials. The significant difference in adsorption capacities demonstrates the superior surface properties and adsorption efficiency of the synthesized CF compared to other materials. The agar-derived CF's exceptional capacity positions it as a promising candidate for efficient pharmaceutical pollutant removal in water treatment applications.

Table 4: Literature comparison of tetracycline adsorption capacity with different carbon-based adsorbents.

| Type of carbon-based adsorbent | $q_e$ (mg $g^{-1}$) | Reference |
|---|---|---|
| CF derived from agar | **1831** | **This work** |

View Article Online
DOI: 10.1039/D5MA00720H



| | | |
|---|---|---|
| Graphene oxide/ZnO | 1590 | 47 |
| Lignin-derived carbon materials (ALUNC-0.5) | 1414 | 48 |
| Magnetic Fe/porous carbon hybrid (MagFePC) | 1301 | 49 |
| FeCo-MOF@$CoFe_2O_4$/porous carbon | 909 | 50 |
| Three-dimensional (3D) framework carbon material with defects | 527 | 51 |
| NaOH-activated carbon | 455 | 39 |
| 3D carbon aerogel (AO-WPC) | 385 | 52 |
| Carbon-$Fe_3C$/lignin composites | 350 | 50 |
| Hazelnut shell derived activated carbon (HSAC) | 302 | 38 |
| Graphene oxide (GO) | 313 | 41 |
| Activated corn straw based porous carbon | 227 | 45 |
| *Pinus taeda*-derived activated biochar | 275 | 53 |
| Rice straw derived biochar | 98 | 35 |
| Hydrochar derived magnetic porous carbon | 25 | 54 |

### *3.1.11. Reusability*

Batch adsorption studies were conducted to evaluate the reusability of the CF adsorbent. After each adsorption cycle, the used adsorbent was separated and thoroughly rinsed with double-distilled water to remove any residual contaminants. To regenerate the adsorbent, it was subjected to a desorption step involving washing with an appropriate desorbing agent, such as ethanol, to facilitate the release of the adsorbed tetracycline. The adsorbent was then rinsed again with double-distilled water and dried at 40 °C in a hot air oven. The adsorption performance of the regenerated adsorbent was evaluated over three consecutive cycles, each with an initial tetracycline concentration of 200 mg $L^{-1}$. The maximum removal efficiencies were found to be 96.2%, 95.6%, and 94.0% for the first, second, and third cycles, respectively, as shown in Figure 10. The slight decline in adsorption capacity over successive cycles can be primarily attributed to the incomplete desorption of tetracycline, particularly within the micropores of the adsorbent, leading to potential

View Article Online
DOI: 10.1039/D5MA00720H



pore blockage and residual chemisorbed species. Indeed, more studies are ongoing to demonstrate the long term stability of the adsorbent as well as in evaluating the structural integrity of these materials.

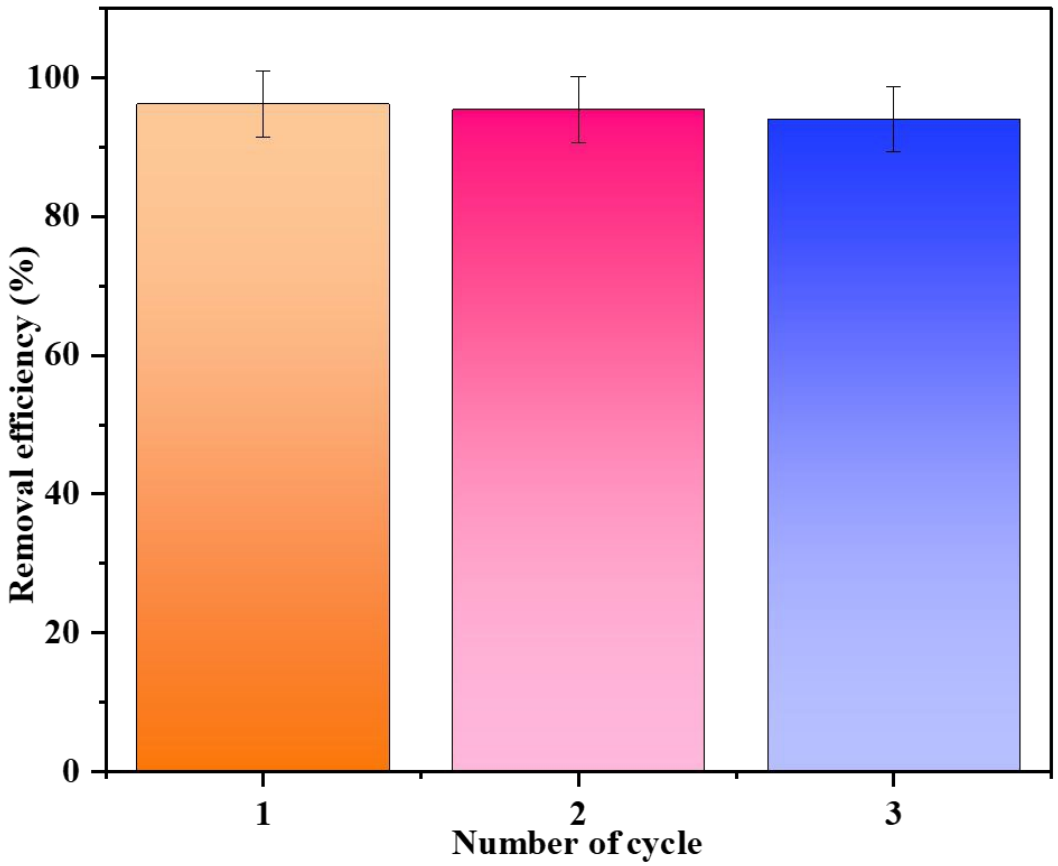


Figure 10: Effect of adsorbent reusability on the removal efficiency of tetracycline. [Experimental conditions: Feed concentrations = 200 mg $L^{-1}$, adsorbent loading = 1 g $L^{-1}$)

### *2.1.12 Adsorption Mechanism:*

The adsorption of tetracycline on ZnO carbon foam occurs through a combination of physical and chemical interactions that work together to achieve high removal efficiency. The CF has a hierarchical porous network, which means there are many accessible pores of different sizes and a high number of available active sites. This structure allows tetracycline molecules to quickly diffuse into the adsorbent and come into close contact with its surface[55]. In the initial stage, tetracycline molecules are attracted to the CF surface through physical adsorption. This is mainly

View Article Online
DOI: 10.1039/D5MA00720H



driven by van der Waals forces, which are weak intermolecular attractions that help bring tetracycline molecules close to the surface. Depending on the pH of the solution, this attraction is enhanced by electrostatic forces between the ionized tetracycline molecules and oppositely charged sites on the CF surface[56,57]. When tetracycline molecules are close to the surface, stronger chemical interactions take place. The carbon domains within CF have delocalized π-electrons that can interact with the aromatic rings of tetracycline through π–π stacking. This type of interaction is common between aromatic compounds and carbon materials. The oxygen-containing functional groups on CF, such as hydroxyl (–OH) and carboxyl (–COOH) groups, can form hydrogen bonds with functional groups in tetracycline, such as its hydroxyl and amide groups. FTIR analysis confirms the presence of these functional groups on CF and shows changes after tetracycline adsorption, indicating hydrogen bonding is involved[58]. Adsorption isotherm and kinetic studies indicate that the overall adsorption mechanism involves a multilayer heterogeneous adsorption, as suggested by the good fit of Freundlich models alongside pseudo-second-order kinetics.

An additional and important mechanism in this system comes from the ZnO nanoparticles embedded in the CF matrix. These ZnO particles act as Lewis's acid sites, meaning they can accept electron pairs from TC's electron-rich groups, such as phenolic and amide functionalities. This forms coordination bonds that further strengthen the adsorption[59,60]. Overall, the main active sites for TC adsorption are the oxygen-containing functional groups on the carbon, the π–electron-rich graphitic domains, and the ZnO nanoparticle surfaces. These work together to give CF its high adsorption capacity.

## 3.2 Material characterization results

### *3.2.1 FTIR analysis*

View Article Online
DOI: 10.1039/D5MA00720H



The choice of biomass precursor and the metal catalyst significantly influences the structure and functional group content of the resulting CF which impacts its applicability. Therefore, FTIR analysis was carried out to determine the presence of different functional groups on the CF. The FTIR spectra of various CF synthesized using a) zinc nitrate catalyzed CF derived from different biomass carbon precursors b) CF derived from agar using different metal nitrate catalysts and the comparison of both fresh and spent zinc-agar based CF adsorbent is shown in Figure 11 (a, b and c). It is evident from Figure 11a that the FTIR spectra of CF derived from different biomass precursors indicates the presence of broad and strong absorption bands in the range of 3600-3800 $cm^{-1}$ which typically correspond to the stretching vibrations of hydroxyl groups. This peak which is noticed in almost all biomass derived CF is mainly due to the incomplete dehydration reaction [61]. The C=O stretching peak noticed at 1639 $cm^{-1}$ is an indicative of carboxyl, ester or ketone functional groups in CF that are formed due to incomplete carbonization. The C=C stretching peak corresponding at 1547 $cm^{-1}$ corresponds to the presence of aromatic compounds formed during foaming process. The peak around 1409 $cm^{-1}$ originates from the O–H in-plane bending vibration [27]. The absorption peak at 1050 $cm^{-1}$ is due to C-O stretching vibration from alcohols, ethers, or ester groups that are common in partially carbonized biomass. The differences in peak intensities and positions among the biomass precursors reflect variations in their chemical compositions. Cellulose and starch show stronger O-H and C-H stretches due to their polysaccharide structures. The weaker C=C peaks in sucrose compared to cellulose may suggest less efficient conversion to aromatic carbon structures.

Each metal nitrate catalyst seems to influence the carbonization pathway differently (Figure 11b). For example, Fe and Cr likely promote more significant graphitization, as seen by the stronger C=C peaks, while Zn and Mg might lead to less efficient carbon structure formation due to weaker

View Article Online
DOI: 10.1039/D5MA00720H

aromatic bands. Metal-oxygen peaks in the range of 500 – 600 $cm^{-1}$ are associated with the formation of metal residues or oxides incorporated during the carbonization process. Tetracycline that has been adsorbed onto CF is mostly responsible for the minor peak alterations that were seen in the fingerprint area of 500–1500 $cm^{-1}$ with the spent adsorbent (Figure 11c).

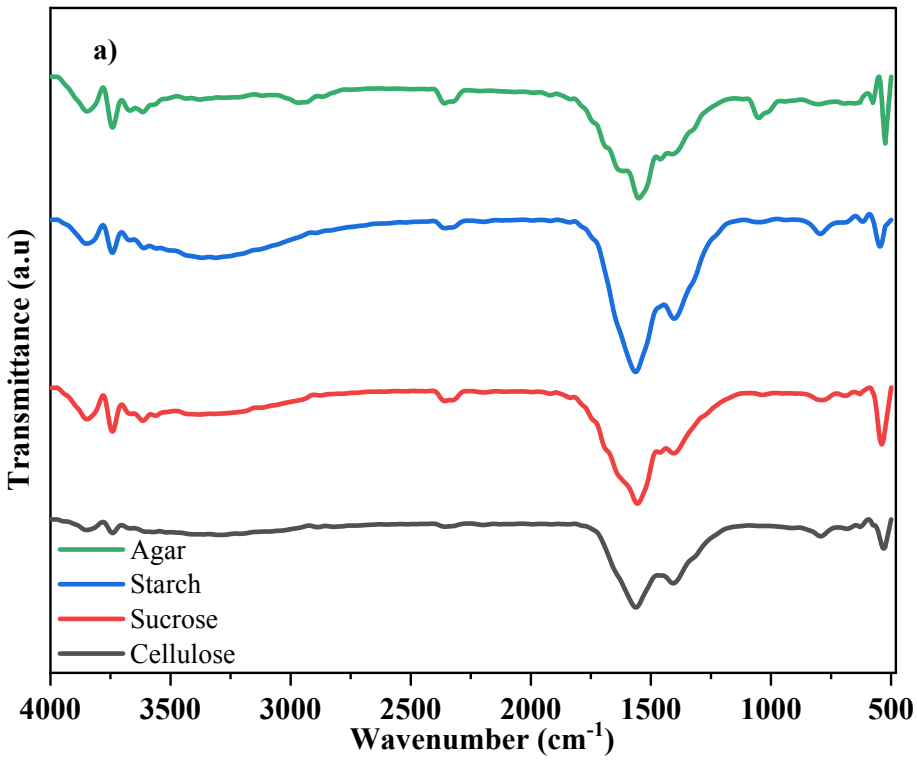

View Article Online
DOI: 10.1039/D5MA00720H



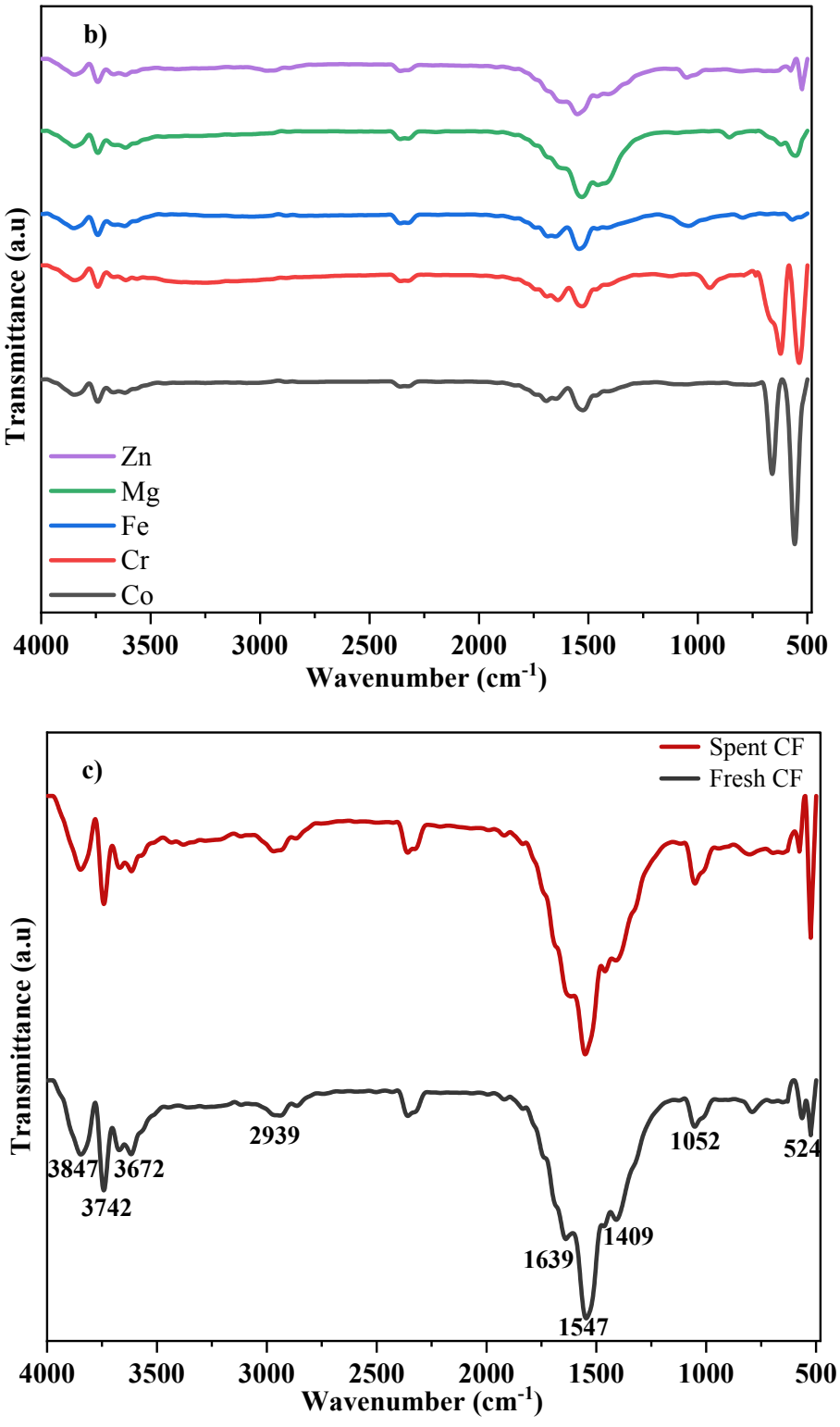


Figure 11: FTIR spectra of **a)** Zinc nitrate catalyzed CF derived from various biomass streams **b)** Agar based CF catalyzed with different metal nitrates **c)** fresh and spent adsorbent of Agar based CF catalyzed with zinc.

View Article Online
DOI: 10.1039/D5MA00720H



### *3.2.2 XRD analysis*

The XRD spectra of fresh and spent CF as depicted in Figure 12. The primary diffraction peaks have been indexed at specific 2θ values: 31.80°, 34.6°, 36.25°, 47.49°, 56.65°, 62.90°, and 68.19° corresponding to the crystallographic planes (100), (002), (101), (102), (110), (103) and (112) of the wurtzite phase of ZnO particles[30]. A weaker signal, attributable to the carbon particles, suggests the amorphous nature of the carbon material. This interpretation is supported by the lack of distinct crystalline peaks in the XRD pattern, indicating that the CF is predominantly amorphous. These crystallite size measurements provide insight into the material's microstructural properties, suggesting a consistent and well-defined crystalline morphology for CF[47,62]. Following the adsorption, the XRD pattern reveals a reduction in the intensity of specific peaks and slight shifts in peak positions. The observed decrease in peak intensity may be due to the adsorption of tetracycline molecules on the surface or within the pores of the CF, leading to partial obstruction of the crystallographic planes and reducing the corresponding diffraction intensity. Potential shifts in peak positions may indicate structural changes or strain introduced by the interaction between ZnO and the adsorbate.

View Article Online
DOI: 10.1039/D5MA00720H



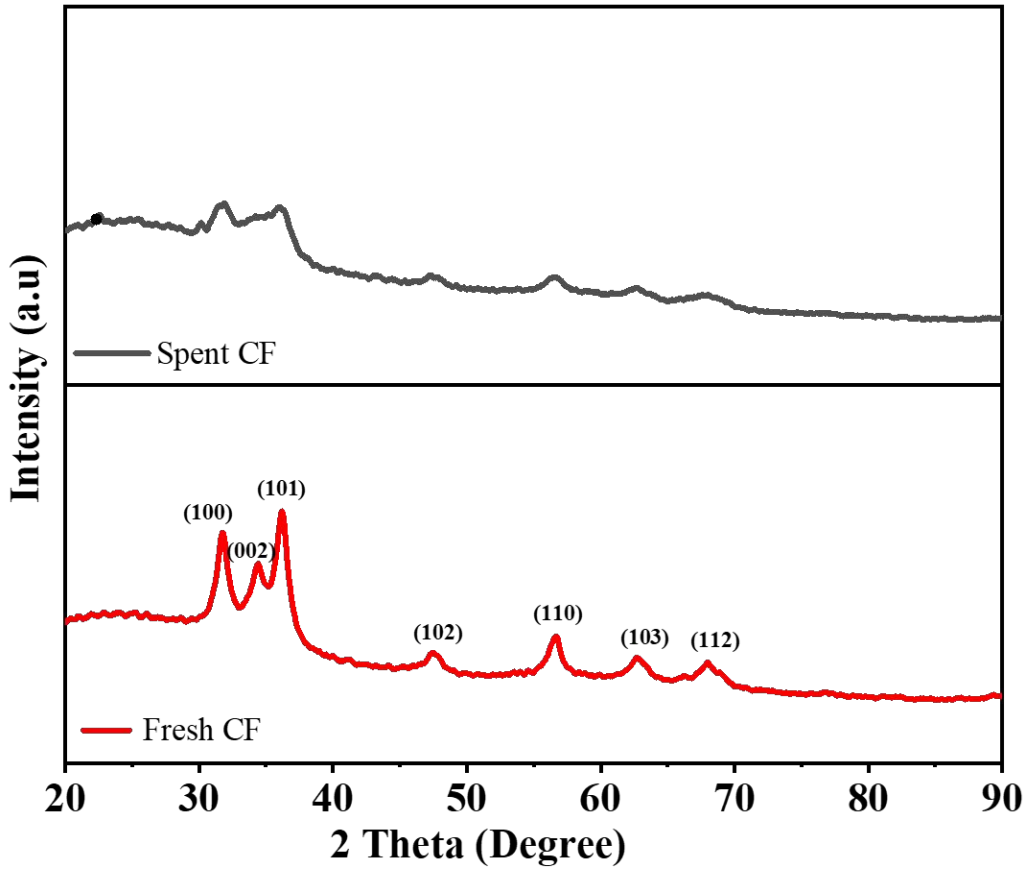


Figure 12: XRD spectra of fresh and spent Zinc catalyzed agar based CF.

### *3.2.3 Surface characteristics*

The surface morphology of both fresh and spent zinc catalyzed CF is shown in Figure 13 a & b. The CF exhibits a porous structure, beneficial for adsorption due to the increased number of active sites. The variation in pore sizes is attributed to gas release from metal nitrate catalysts during biomass carbonization at elevated temperatures, which contributes to the foaming process and results in larger pores. Similar observations were reported[30] during CF synthesis from starch, leading to larger pore formation. While it is clear that the spent adsorbent is not as porous in nature as the fresh adsorbent indicating the pore blocking due to the deposition of the organics after adsorption.

View Article Online
DOI: 10.1039/D5MA00720H



Energy-dispersive X-ray spectroscopy (EDX) analysis confirmed the presence of zinc, oxygen, and carbon in the samples (Figure 13 c & d). The fresh CF adsorbent contained approximately 60% zinc, 19% carbon, and 21% oxygen. After tetracycline adsorption, the carbon content increased to 40%, indicating the presence of adsorbed organics, while the zinc content decreased to 30%, and oxygen increased to 30%, signifying successful adsorption onto the zinc catalyzed CF[63].

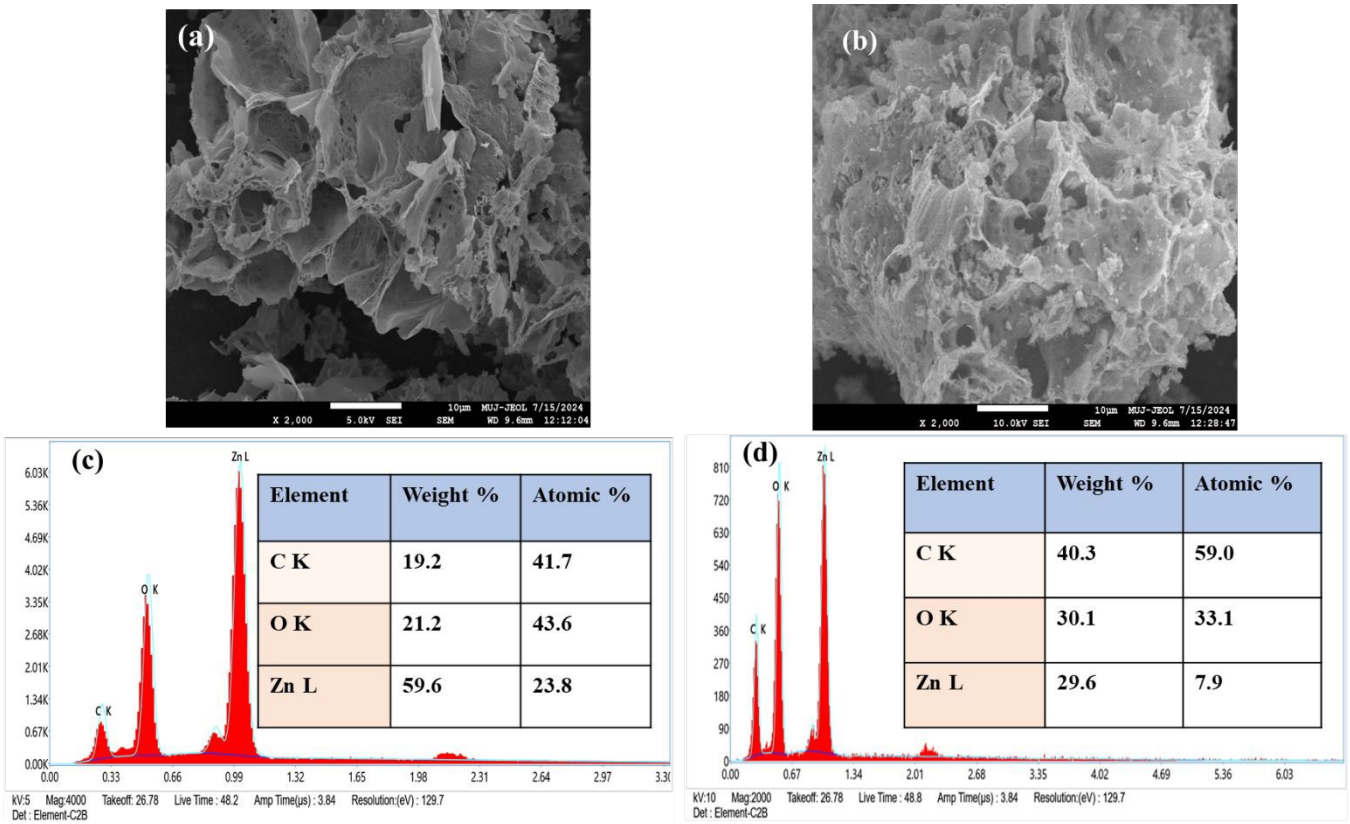


Figure 13: FESEM and EDX analysis of fresh (a, c) and spent adsorbent (b, d) with elemental composition tabulated.

### *3.3.3 BET Analysis:*

The porous structure of the modified carbon foam was systematically investigated using nitrogen adsorption–desorption isotherms. The Brunauer–Emmett–Teller (BET) analysis revealed a specific surface area of 38.09 $m^2/g$, representing the total accessible external surface area for

View Article Online
DOI: 10.1039/D5MA00720H



adsorption. Further analysis using the Barrett–Joyner–Halenda (BJH) method indicated a mesopore surface area of 74.10 $m^2/g$, along with a total pore volume of 0.058 $cm^3/g$ and an average pore diameter of 1.69 nm. Although this pore width falls at the lower boundary of the mesoporous regime (2–50 nm), it also suggests a significant contribution from micropores. To confirm this, the Horváth–Kawazoe (HK) method was employed, which yielded a micropore volume of 0.024 $cm^3/g$, thereby substantiating the coexistence of both micro- and mesopores within the foam. Such a hierarchical pore structure, combining micropores (which provide high adsorption potential due to strong adsorbate–adsorbent interactions) and mesopores (which facilitate molecular diffusion and accessibility), is advantageous for adsorption processes. The relatively modest BET surface area compared to commercial activated carbons is compensated by the presence of interconnected pores and high adsorption affinity, which together explain the exceptionally high adsorption capacity observed for the synthesized carbon foam[64,65].

View Article Online
DOI: 10.1039/D5MA00720H



## 4. Conclusion

This study successfully demonstrates the synthesis of CF from various biomass-derived precursors, showing high adsorption capacity for pharmaceutical effluent removal. Despite the use of different biomass precursors—agar, cellulose, sucrose, and starch—the adsorption efficiency for tetracycline remained consistent, indicating that the carbon precursor plays a limited role in adsorption performance. However, the catalytic influence of different metal nitrates was significant. In particular, zinc-catalyzed CF derived from agar exhibited complete removal of a range of pharmaceutical contaminants, highlighting its superior adsorption potential. Tetracycline adsorption followed the Freundlich isotherm, suggesting that the CF have heterogeneous surfaces with multiple adsorption sites, leading to non-uniform adsorbate distribution. The kinetics of the adsorption process adhered to a pseudo-second-order model, confirming chemisorption as the dominant mechanism. Thermodynamic analyses further revealed that the adsorption is spontaneous and endothermic, driven by entropy increase, making the process favorable under the tested conditions. A key finding of this work is the excellent reusability of the zinc-catalyzed CF, which retained its high adsorption capacity across multiple cycles without significant loss of efficiency. This highlights its potential as a cost-effective and sustainable solution for water treatment applications, offering both environmental and economic benefits in the management of pharmaceutical pollutants.

View Article Online
DOI: 10.1039/D5MA00720H



## Acknowledgments

The authors would like to thank Manipal University Jaipur (MUJ) for providing access to the Central Analytical Facilities (CAF) and Sophisticated Analytical Instrumentation Facility (SAIF). AGC and PKS would like to acknowledge the Manipal Research Board, Manipal, India for providing financial support to facilitate the study.

## Credit authorship contribution statement

**Meena Choudhary**: Investigation, Methodology Data curation, Writing - original draft; **Nandana Chakinala**: Formal analysis, Software, Validation, Supervision, Writing - review & editing; **Pooja Saini**: Formal analysis, Writing - review & editing; **Praveen K. Surolia**: Supervision, Writing - review & editing; **Anand G. Chakinala**: Conceptualization, Project administration, Validation, Supervision, Writing - review & editing.

## Funding

This research did not receive any specific grant from funding agencies in the public, commercial, or not-for-profit sectors.

## Declarations

## Data availability

The data that support this study are available from the corresponding author upon request.

## Competing interests

The authors have no relevant financial or non-financial interests to disclose.

View Article Online
DOI: 10.1039/D5MA00720H



## Reference

(1) Deletic, A.; Wang, H. Water Pollution Control for Sustainable Development. *Engineering* **2019**, *5* (5), 839–840. https://doi.org/10.1016/j.eng.2019.07.013.

(2) Kovalakova, P.; Cizmas, L.; McDonald, T. J.; Marsalek, B.; Feng, M.; Sharma, V. K. Occurrence and Toxicity of Antibiotics in the Aquatic Environment: A Review. *Chemosphere* **2020**, *251*, 126351. https://doi.org/10.1016/j.chemosphere.2020.126351.

(3) Wang, T.; Pan, X.; Ben, W.; Wang, J.; Hou, P.; Qiang, Z. Adsorptive Removal of Antibiotics from Water Using Magnetic Ion Exchange Resin. *J. Environ. Sci. (China)* **2017**, *52*, 111–117. https://doi.org/10.1016/j.jes.2016.03.017.

(4) Zhang, S.; Gao, H.; Xu, X.; Cao, R.; Yang, H.; Xu, X.; Li, J. MOF-Derived CoN/N-C@SiO2 Yolk-Shell Nanoreactor with Dual Active Sites for Highly Efficient Catalytic Advanced Oxidation Processes. *Chem. Eng. J.* **2020**, *381* (June 2019), 122670. https://doi.org/10.1016/j.cej.2019.122670.

(5) Dai, Y.; Li, J.; Shan, D. Adsorption of Tetracycline in Aqueous Solution by Biochar Derived from Waste Auricularia Auricula Dregs. *Chemosphere* **2020**, *238*, 124432. https://doi.org/10.1016/j.chemosphere.2019.124432.

(6) No Title. https://doi.org/https://doi.org/10.1021/es803268b.

(7) Yang, J.; Dou, Y.; Yang, H.; Wang, D. A Novel Porous Carbon Derived from CO2 for High-Efficient Tetracycline Adsorption: Behavior and Mechanism. *Appl. Surf. Sci.* **2021**, *538* (September 2020), 148110. https://doi.org/10.1016/j.apsusc.2020.148110.

(8) Ma, J.; Jiang, Z.; Cao, J.; Yu, F. Enhanced Adsorption for the Removal of Antibiotics by Carbon Nanotubes/Graphene Oxide/Sodium Alginate Triple-Network Nanocomposite Hydrogels in Aqueous Solutions. *Chemosphere* **2020**, *242*, 125188. https://doi.org/10.1016/j.chemosphere.2019.125188.

View Article Online
DOI: 10.1039/D5MA00720H



(9) da Silva Alves, D. C.; Healy, B.; Pinto, L. A. d. A.; Cadaval, T. R. S.; Breslin, C. B. Recent Developments in Chitosan-Based Adsorbents for the Removal of Pollutants from Aqueous Environments. *Molecules* **2021**, *26* (3). https://doi.org/10.3390/molecules26030594.

(10) Isaeva, V. I.; Vedenyapina, M. D.; Kurmysheva, A. Y.; Weichgrebe, D.; Nair, R. R.; Nguyen, N. P. T.; Kustov, L. M. Modern Carbon–Based Materials for Adsorptive Removal of Organic and Inorganic Pollutants from Water and Wastewater. *Molecules* **2021**, *26* (21), 1–95. https://doi.org/10.3390/molecules26216628.

(11) Han, H.; Rafiq, M. K.; Zhou, T.; Xu, R.; Mašek, O.; Li, X. A Critical Review of Clay-Based Composites with Enhanced Adsorption Performance for Metal and Organic Pollutants. *J. Hazard. Mater.* **2019**, *369* (January), 780–796. https://doi.org/10.1016/j.jhazmat.2019.02.003.

(12) Xiang, Y.; Xu, Z.; Wei, Y.; Zhou, Y.; Yang, X.; Yang, Y.; Yang, J.; Zhang, J.; Luo, L.; Zhou, Z. Carbon-Based Materials as Adsorbent for Antibiotics Removal: Mechanisms and Influencing Factors. *J. Environ. Manage.* **2019**, *237* (January), 128–138. https://doi.org/10.1016/j.jenvman.2019.02.068.

(13) Chen, S.; He, G.; Hu, H.; Jin, S.; Zhou, Y.; He, Y.; He, S.; Zhao, F.; Hou, H. Elastic Carbon Foam via Direct Carbonization of Polymer Foam for Flexible Electrodes and Organic Chemical Absorption. *Energy Environ. Sci.* **2013**, *6* (8), 2435–2439. https://doi.org/10.1039/c3ee41436a.

(14) Lee, C. G.; Song, M. K.; Ryu, J. C.; Park, C.; Choi, J. W.; Lee, S. H. Application of Carbon Foam for Heavy Metal Removal from Industrial Plating Wastewater and Toxicity Evaluation of the Adsorbent. *Chemosphere* **2016**, *153*, 1–9.

View Article Online
DOI: 10.1039/D5MA00720H



https://doi.org/10.1016/j.chemosphere.2016.03.034.

(15) Stojanovska, E.; Calisir, M. D.; Ozturk, N. D.; Kilic, A. *Carbon-Based Foams: Preparation and Applications*; Elsevier Ltd., 2018. https://doi.org/10.1016/B978-0-08-102509-3.00003-1.

(16) Zhang, S. P.; Liu, M. X.; Gan, L. H.; Wu, F. R.; Xu, Z. J.; Hao, Z. X.; Chen, L. W. Synthesis of Carbon Foams with a High Compressive Strength from Arylacetylene. *Xinxing Tan Cailiao/ New Carbon Mater.* **2010**, *25* (1), 9–14. https://doi.org/10.1016/S1872-5805(09)60012-3.

(17) Li, W.; Huang, Z.; Wu, Y.; Zhao, X.; Liu, S. Honeycomb Carbon Foams with Tunable Pore Structures Prepared from Liquefied Larch Sawdust by Self-Foaming. *Ind. Crops Prod.* **2015**, *64* (1), 215–223. https://doi.org/10.1016/j.indcrop.2014.09.043.

(18) García, R.; Rodríguez, E.; Díez, M. A.; Arenillas, A.; Villanueva, S. F.; Rey-Raap, N.; Cuesta, C.; López-Antón, M. A.; Martínez-Tarazona, M. R. Synthesis of Micro- and Mesoporous Carbon Foams with Nanodispersed Metals for Adsorption and Catalysis Applications. *Materials (Basel).* **2023**, *16* (4). https://doi.org/10.3390/ma16041336.

(19) Prabhakaran, K.; Singh, P. K.; Gokhale, N. M.; Sharma, S. C. Processing of Sucrose to Low Density Carbon Foams. *J. Mater. Sci.* **2007**, *42* (11), 3894–3900. https://doi.org/10.1007/s10853-006-0481-1.

(20) Wang, C.; O'Connell, M. J.; Chan, C. K. Facile One-Pot Synthesis of Highly Porous Carbon Foams for High-Performance Supercapacitors Using Template-Free Direct Pyrolysis. *ACS Appl. Mater. Interfaces* **2015**, *7* (16), 8952–8960. https://doi.org/10.1021/acsami.5b02453.

(21) Zang, J.; Wu, T.; Song, H.; Zhou, N.; Fan, S.; Xie, Z.; Tang, J. Removal of Tetracycline

View Article Online
DOI: 10.1039/D5MA00720H



by Hydrous Ferric Oxide: Adsorption Kinetics, Isotherms, and Mechanism. *Int. J. Environ. Res. Public Health* **2019**, *16* (22). https://doi.org/10.3390/ijerph16224580.

(22) Emrooz, H. B. M.; Aghdaee, A. A.; Rostami, M. R. Zinc-Salt Assisted Synthesis of Three-Dimensional Oxygen and Nitrogen Co-Doped Hierarchical Micro-Meso Porous Carbon Foam for Supercapacitors. *Sci. Rep.* **2021**, *11* (1), 21798. https://doi.org/10.1038/s41598-021-01151-3.

(23) Varila, T.; Romar, H.; Lassi, U. Catalytic Effect of Transition Metals (Copper, Iron, and Nickel) on the Foaming and Properties of Sugar-Based Carbon Foams. *Top. Catal.* **2019**, *62* (7–11). https://doi.org/10.1007/s11244-019-01171-4.

(24) Zhang, Y.; Wang, Q.; Li, R.; Lou, Z.; Li, Y. A Novel Phenolic Foam-Derived Magnetic Carbon Foam Treated as Adsorbent for Rhodamine B: Characterization and Adsorption Kinetics. *Crystals* **2020**, *10* (3). https://doi.org/10.3390/cryst10030159.

(25) Zhang, X.; Lin, L.; Gao, W.; Zhou, Y.; Lin, Q. A Novel Fe-Containing Carbon Foam with Hierarchical Porous Structure for Efficient Removal of Organic Dyes. *Diam. Relat. Mater.* **2023**, *140*. https://doi.org/10.1016/j.diamond.2023.110492.

(26) Liu, H.; Zhang, J.; Ngo, H. H.; Guo, W.; Wu, H.; Cheng, C.; Guo, Z.; Zhang, C. Carbohydrate-Based Activated Carbon with High Surface Acidity and Basicity for Nickel Removal from Synthetic Wastewater. *RSC Adv.* **2015**, *5* (64). https://doi.org/10.1039/c5ra08987e.

(27) Li, Z.; Xu, J.; Sun, D.; Lin, T.; Huang, F. Nanoporous Carbon Foam for Water and Air Purification. *ACS Appl. Nano Mater.* **2020**, *3* (2), 1564–1570. https://doi.org/10.1021/acsanm.9b02347.

(28) Wang, W.; Gao, M.; Cao, M.; Liu, X.; Yang, H.; Li, Y. A Series of Novel Carbohydrate-

View Article Online
DOI: 10.1039/D5MA00720H



Based Carbon Adsorbents Were Synthesized by Self-Propagating Combustion for Tetracycline Removal. *Bioresour. Technol.* **2021**, *332*, 125059. https://doi.org/10.1016/J.BIORTECH.2021.125059.

(29) Zhang, X.; Wang, K.; He, C.; Lin, Y.; Hu, H.; Huang, Q.; Yu, H.; Zhou, T.; Lin, Q. Regulation Pore Size Distribution for Facilitating Malachite Green Removal on Carbon Foam. *Environ. Res.* **2022**, *213*, 113715. https://doi.org/10.1016/j.envres.2022.113715.

(30) Priyanka, M.; Saravanakumar, M. P. Ultrahigh Adsorption Capacity of Starch Derived Zinc Based Carbon Foam for Adsorption of Toxic Dyes and Its Preliminary Investigation on Oil-Water Separation. *J. Clean. Prod.* **2018**, *197*, 511–524. https://doi.org/10.1016/j.jclepro.2018.06.197.

(31) Saini, P.; Chakinala, N.; Surolia, P. K.; Gupta Chakinala, A. Ultrasound-Assisted Enhanced Adsorption of Textile Dyes with Metal Organic Frameworks. *Sep. Purif. Technol.* **2025**, *354*, 128730. https://doi.org/10.1016/J.SEPPUR.2024.128730.

(32) Wang, T.; Xue, L.; Liu, Y.; Fang, T.; Zhang, L.; Xing, B. Insight into the Significant Contribution of Intrinsic Defects of Carbon-Based Materials for the Efficient Removal of Tetracycline Antibiotics. *Chem. Eng. J.* **2022**, *435*, 134822. https://doi.org/10.1016/j.cej.2022.134822.

(33) Tian, L.; Zhang, L.; Zheng, L.; Chen, Y.; Ding, L.; Fan, J.; Wu, D.; Zou, J.; Luo, S. Overcoming Electrostatic Interaction via Strong Complexation for Highly Selective Reduction of CN − into N 2. *Angew. Chemie Int. Ed.* **2022**, *61* (50). https://doi.org/10.1002/anie.202214145.

(34) Ahamad, T.; Naushad, M.; Al-Shahrani, T.; Al-hokbany, N.; Alshehri, S. M. Preparation of Chitosan Based Magnetic Nanocomposite for Tetracycline Adsorption: Kinetic and

View Article Online
DOI: 10.1039/D5MA00720H



Thermodynamic Studies. *Int. J. Biol. Macromol.* **2020**, *147*, 258–267. https://doi.org/10.1016/j.ijbiomac.2020.01.025.

(35) Dai, J.; Meng, X.; Zhang, Y.; Huang, Y. Effects of Modification and Magnetization of Rice Straw Derived Biochar on Adsorption of Tetracycline from Water. *Bioresour. Technol.* **2020**, *311* (April), 123455. https://doi.org/10.1016/j.biortech.2020.123455.

(36) Ma, J.; Lei, Y.; Khan, M. A.; Wang, F.; Chu, Y.; Lei, W.; Xia, M.; Zhu, S. Adsorption Properties, Kinetics & Thermodynamics of Tetracycline on Carboxymethyl-Chitosan Reformed Montmorillonite. *Int. J. Biol. Macromol.* **2019**, *124*, 557–567. https://doi.org/10.1016/j.ijbiomac.2018.11.235.

(37) Feng, Y.; Yang, F.; Wang, Y.; Ma, L.; Wu, Y.; Kerr, P. G.; Yang, L. Basic Dye Adsorption onto an Agro-Based Waste Material - Sesame Hull (Sesamum Indicum L.). *Bioresour. Technol.* **2011**, *102* (22), 10280–10285. https://doi.org/10.1016/j.biortech.2011.08.090.

(38) Fan, H. T.; Shi, L. Q.; Shen, H.; Chen, X.; Xie, K. P. Equilibrium, Isotherm, Kinetic and Thermodynamic Studies for Removal of Tetracycline Antibiotics by Adsorption onto Hazelnut Shell Derived Activated Carbons from Aqueous Media. *RSC Adv.* **2016**, *6* (111), 109983–109991. https://doi.org/10.1039/c6ra23346e.

(39) Martins, A. C.; Pezoti, O.; Cazetta, A. L.; Bedin, K. C.; Yamazaki, D. A. S.; Bandoch, G. F. G.; Asefa, T.; Visentainer, J. V.; Almeida, V. C. Removal of Tetracycline by NaOH-Activated Carbon Produced from Macadamia Nut Shells: Kinetic and Equilibrium Studies. *Chem. Eng. J.* **2015**, *260*, 291–299. https://doi.org/10.1016/j.cej.2014.09.017.

(40) Chen, Y.; Wang, F.; Duan, L.; Yang, H.; Gao, J. Tetracycline Adsorption onto Rice Husk Ash, an Agricultural Waste: Its Kinetic and Thermodynamic Studies. *J. Mol. Liq.* **2016**,

View Article Online
DOI: 10.1039/D5MA00720H

*222*, 487–494. https://doi.org/10.1016/j.molliq.2016.07.090.

(41) Gao, Y.; Li, Y.; Zhang, L.; Huang, H.; Hu, J.; Shah, S. M.; Su, X. Adsorption and Removal of Tetracycline Antibiotics from Aqueous Solution by Graphene Oxide. *J. Colloid Interface Sci.* **2012**, *368* (1), 540–546. https://doi.org/10.1016/j.jcis.2011.11.015.

(42) Yousef, R. I.; El-Eswed, B.; Al-Muhtaseb, A. H. Adsorption Characteristics of Natural Zeolites as Solid Adsorbents for Phenol Removal from Aqueous Solutions: Kinetics, Mechanism, and Thermodynamics Studies. *Chem. Eng. J.* **2011**, *171* (3), 1143–1149. https://doi.org/10.1016/j.cej.2011.05.012.

(43) Liu, S.; Pan, M.; Feng, Z.; Qin, Y.; Wang, Y.; Tan, L.; Sun, T. Ultra-High Adsorption of Tetracycline Antibiotics on Garlic Skin-Derived Porous Biomass Carbon with High Surface Area. *New J. Chem.* **2020**, *44* (3), 1097–1106. https://doi.org/10.1039/c9nj05396d.

(44) Foo, K. Y.; Hameed, B. H. Insights into the Modeling of Adsorption Isotherm Systems. *Chem. Eng. J.* **2010**, *156* (1), 2–10. https://doi.org/10.1016/j.cej.2009.09.013.

(45) Yang, Q.; Wu, P.; Liu, J.; Rehman, S.; Ahmed, Z.; Ruan, B.; Zhu, N. Batch Interaction of Emerging Tetracycline Contaminant with Novel Phosphoric Acid Activated Corn Straw Porous Carbon: Adsorption Rate and Nature of Mechanism. *Environ. Res.* **2020**, *181* (September), 108899. https://doi.org/10.1016/j.envres.2019.108899.

(46) Yang, G.; Gao, Q.; Yang, S.; Yin, S.; Cai, X.; Yu, X.; Zhang, S.; Fang, Y. Strong Adsorption of Tetracycline Hydrochloride on Magnetic Carbon-Coated Cobalt Oxide Nanoparticles. *Chemosphere* **2020**, *239*, 124831. https://doi.org/10.1016/j.chemosphere.2019.124831.

(47) Qiao, D.; Li, Z.; Duan, J.; He, X. Adsorption and Photocatalytic Degradation Mechanism

View Article Online
DOI: 10.1039/D5MA00720H



of Magnetic Graphene Oxide/ZnO Nanocomposites for Tetracycline Contaminants. *Chem. Eng. J.* **2020**, *400* (April), 125952. https://doi.org/10.1016/j.cej.2020.125952.

(48) Fu, F.; Bai, D.; Cai, Z.; Lin, X.; Qiu, X. Regulating the Porous Structure of Lignin-Derived Carbon Materials for High Adsorption Performance via Dual Nitrogen Source-Assisted Activation. *Ind. Eng. Chem. Res.* **2024**, *63* (29), 12938–12949. https://doi.org/10.1021/acs.iecr.4c01835.

(49) Gu, W.; Huang, X.; Tian, Y.; Cao, M.; Zhou, L.; Zhou, Y.; Lu, J.; Lei, J.; Zhou, Y.; Wang, L.; Liu, Y.; Zhang, J. High-Efficiency Adsorption of Tetracycline by Cooperation of Carbon and Iron in a Magnetic Fe/Porous Carbon Hybrid with Effective Fenton Regeneration. *Appl. Surf. Sci.* **2021**, *538*. https://doi.org/10.1016/j.apsusc.2020.147813.

(50) Jiang, Y. C.; Luo, M. F.; Niu, Z. N.; Xu, S. Y.; Gao, Y.; Gao, Y.; Gao, W. J.; Luo, J. J.; Liu, R. L. In-Situ Growth of Bimetallic FeCo-MOF on Magnetic Biochar for Enhanced Clearance of Tetracycline and Fruit Preservation. *Chem. Eng. J.* **2023**, *451*. https://doi.org/10.1016/j.cej.2022.138804.

(51) Wang, T.; Xue, L.; Liu, Y.; Fang, T.; Zhang, L.; Xing, B. Insight into the Significant Contribution of Intrinsic Defects of Carbon-Based Materials for the Efficient Removal of Tetracycline Antibiotics. *Chem. Eng. J.* **2022**, *435*. https://doi.org/10.1016/j.cej.2022.134822.

(52) Ma, L.; Li, D.; Chen, X.; Xu, H.; Tian, Y. A Sustainable Carbon Aerogel from Waste Paper with Exceptional Performance for Antibiotics Removal from Water. *J. Hazard. Mater.* **2024**, *474*, 134738. https://doi.org/10.1016/j.jhazmat.2024.134738.

(53) Jang, H. M.; Yoo, S.; Choi, Y. K.; Park, S.; Kan, E. Adsorption Isotherm, Kinetic Modeling and Mechanism of Tetracycline on Pinus Taeda-Derived Activated Biochar.

View Article Online
DOI: 10.1039/D5MA00720H



*Bioresour. Technol.* **2018**, *259* (January), 24–31. https://doi.org/10.1016/j.biortech.2018.03.013.

(54) Zhu, X.; Liu, Y.; Qian, F.; Zhou, C.; Zhang, S.; Chen, J. Preparation of Magnetic Porous Carbon from Waste Hydrochar by Simultaneous Activation and Magnetization for Tetracycline Removal. *Bioresour. Technol.* **2014**, *154*, 209–214. https://doi.org/10.1016/j.biortech.2013.12.019.

(55) Dai, Y.; Li, J.; Shan, D. Adsorption of Tetracycline in Aqueous Solution by Biochar Derived from Waste Auricularia Auricula Dregs. *Chemosphere* **2020**, *238*, 124432. https://doi.org/10.1016/j.chemosphere.2019.124432.

(56) Zhao, C.; Ma, J.; Li, Z.; Xia, H.; Liu, H.; Yang, Y. Highly Enhanced Adsorption Performance of Tetracycline Antibiotics on KOH-Activated Biochar Derived from Reed Plants. *RSC Adv.* **2020**, *10* (9), 5066–5076. https://doi.org/10.1039/C9RA09208K.

(57) Jang, H. M.; Yoo, S.; Choi, Y.-K.; Park, S.; Kan, E. Adsorption Isotherm, Kinetic Modeling and Mechanism of Tetracycline on Pinus Taeda-Derived Activated Biochar. *Bioresour. Technol.* **2018**, *259*, 24–31. https://doi.org/10.1016/j.biortech.2018.03.013.

(58) Yang, J.; Dou, Y.; Yang, H.; Wang, D. A Novel Porous Carbon Derived from CO2 for High-Efficient Tetracycline Adsorption: Behavior and Mechanism. *Appl. Surf. Sci.* **2021**, *538*, 148110. https://doi.org/10.1016/j.apsusc.2020.148110.

(59) Oliveira, C.; de Oliveira, A. L. M.; Chantelle, L.; Landers, R.; Medina-Carrasco, S.; Del Mar Orta, M.; Silva Filho, E. C.; Fonseca, M. G. Zinc (II) Modified Hydroxyapatites for Tetracycline Removal: Zn (II) Doping or ZnO Deposition and Their Influence in the Adsorption. *Polyhedron* **2021**, *194*, 114879. https://doi.org/10.1016/j.poly.2020.114879.

(60) Wang, W.; Gao, M.; Cao, M.; Liu, X.; Yang, H.; Li, Y. A Series of Novel Carbohydrate-

View Article Online
DOI: 10.1039/D5MA00720H



Based Carbon Adsorbents Were Synthesized by Self-Propagating Combustion for Tetracycline Removal. *Bioresour. Technol.* **2021**, *332*, 125059. https://doi.org/10.1016/j.biortech.2021.125059.

(61) Li, J.; Zhao, Z.; Li, D.; Tang, X.; Feng, H.; Qi, W.; Wang, Q. Multifunctional Walnut Shell Layer Used for Oil/Water Mixtures Separation and Dyes Adsorption. *Appl. Surf. Sci.* **2017**, *419*, 869–874. https://doi.org/10.1016/j.apsusc.2017.05.114.

(62) Zhang, Q.; Li, J.; Lin, Q.; Fang, C. A Stiff ZnO/Carbon Foam Composite with Second-Level Macroporous Structure Filled ZnO Particles for Heavy Metal Ions Removal. *Environ. Res.* **2020**, *188* (November 2019), 109698. https://doi.org/10.1016/j.envres.2020.109698.

(63) Zhang, F.; Chen, X.; Wu, F.; Ji, Y. High Adsorption Capability and Selectivity of ZnO Nanoparticles for Dye Removal. *Colloids Surfaces A Physicochem. Eng. Asp.* **2016**, *509*, 474–483. https://doi.org/10.1016/j.colsurfa.2016.09.059.

(64) Lee, C.-G.; Lee, S.; Park, J.-A.; Park, C.; Lee, S. J.; Kim, S.-B.; An, B.; Yun, S.-T.; Lee, S.-H.; Choi, J.-W. Removal of Copper, Nickel and Chromium Mixtures from Metal Plating Wastewater by Adsorption with Modified Carbon Foam. *Chemosphere* **2017**, *166*, 203–211. https://doi.org/10.1016/j.chemosphere.2016.09.093.

(65) Lee, C.-G.; Jeon, J.-W.; Hwang, M.-J.; Ahn, K.-H.; Park, C.; Choi, J.-W.; Lee, S.-H. Lead and Copper Removal from Aqueous Solutions Using Carbon Foam Derived from Phenol Resin. *Chemosphere* **2015**, *130*, 59–65. https://doi.org/10.1016/j.chemosphere.2015.02.055.

View Article Online
DOI: 10.1039/D5MA00720H

924



View Article Online
DOI: 10.1039/D5MA00720H

## Data Availability Statement

The data that support this study are available from the corresponding author upon request.

## Credit authorship contribution statement

**Meena Choudhary**: Investigation, Methodology Data curation, Writing - original draft; **Nandana Chakinala**: Formal analysis, Software, Validation, Supervision, Writing - review & editing; **Pooja Saini**: Formal analysis, Writing - original draft; **Praveen K. Surolia**: Supervision, Writing - review & editing; **Anand G. Chakinala**: Conceptualization, Project administration, Validation, Supervision, Writing - review & editing.